Cell Reports

Article

Non-steroidal Anti-inflammatory Drugs Target TWISTED DWARF1-Regulated Actin Dynamics and Auxin Transport-Mediated Plant Development

Graphical Abstract

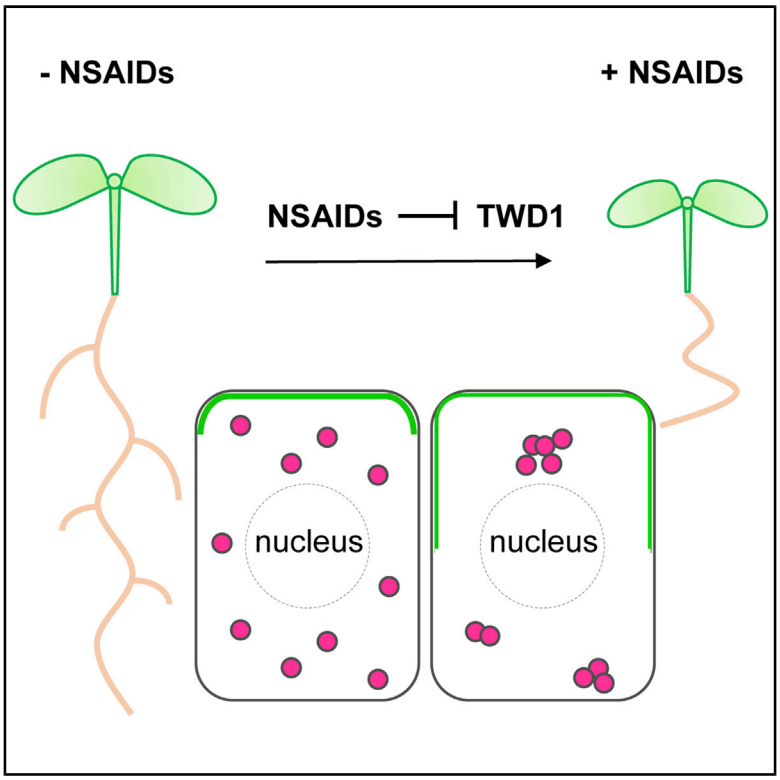

Highlights

- NSAIDs exhibit striking activity in shaping *Arabidopsis* root development
- NSAIDs interfere with auxin transport and endomembrane trafficking
- NSAID treatments impair actin filament dynamics and endosomal mobility
- NSAIDs directly target TWD1, suppressing its chaperone activity and actin dynamics

Authors

Shutang Tan, Martin Di Donato, Matouš Glanc, ..., Jan Petrášek, Markus Geisler, Jiří Friml

Correspondence

jiri.friml@ist.ac.at

In Brief

Non-steroidal anti-inflammatory drugs (NSAIDs) are based on the phytohormone salicylic acid, but there are few studies investigating their bioactivities in plants. Tan et al. show that NSAIDs modulate *Arabidopsis* root development via directly binding to the immunophilin protein TWD1 and hence regulate its chaperone activity and endomembrane trafficking.

Tan et al., 2020, Cell Reports *33*, 108463
December 1, 2020
https://doi.org/10.1016/j.celrep.2020.108463

CellPress

Cell Reports

CellPress
OPEN ACCESS

Article

Non-steroidal Anti-inflammatory Drugs Target TWISTED DWARF1-Regulated Actin Dynamics and Auxin Transport-Mediated Plant Development

Shutang Tan,[1] Martin Di Donato,[2] Matouš Glanc,[1,3] Xixi Zhang,[1,4] Petr Klíma,[5] Jie Liu,[2] Aurélien Bailly,[6] Noel Ferro,[7] Jan Petrášek,[3,5] Markus Geisler,[2] and Jiří Friml[1,8,*]

[1]Institute of Science and Technology Austria (IST Austria), Am Campus 1, 3400 Klosterneuburg, Austria
[2]Department of Biology, University of Fribourg, 1700 Fribourg, Switzerland
[3]Department of Experimental Plant Biology, Faculty of Science, Charles University, Viničná 5, 128 43 Prague 2, Czech Republic
[4]Department of Applied Genetics and Cell Biology, University of Natural Resources and Life Sciences (BOKU), Muthgasse 18, 1190 Vienna, Austria
[5]The Czech Academy of Sciences, Institute of Experimental Botany, Rozvojová 263, 165 02 Prague 6, Czech Republic
[6]Department of Plant and Microbial Biology, University of Zurich, 8008 Zurich, Switzerland
[7]University of Bonn, Mulliken Center for Theoretical Chemistry, Institute for Physical and Theoretical Chemistry, 53115 Bonn, Germany
[8]Lead Contact
*Correspondence: jiri.friml@ist.ac.at
https://doi.org/10.1016/j.celrep.2020.108463

SUMMARY

The widely used non-steroidal anti-inflammatory drugs (NSAIDs) are derivatives of the phytohormone salicylic acid (SA). SA is well known to regulate plant immunity and development, whereas there have been few reports focusing on the effects of NSAIDs in plants. Our studies here reveal that NSAIDs exhibit largely overlapping physiological activities to SA in the model plant *Arabidopsis*. NSAID treatments lead to shorter and agravitropic primary roots and inhibited lateral root organogenesis. Notably, in addition to the SA-like action, which in roots involves binding to the protein phosphatase 2A (PP2A), NSAIDs also exhibit PP2A-independent effects. Cell biological and biochemical analyses reveal that many NSAIDs bind directly to and inhibit the chaperone activity of TWISTED DWARF1, thereby regulating actin cytoskeleton dynamics and subsequent endosomal trafficking. Our findings uncover an unexpected bioactivity of human pharmaceuticals in plants and provide insights into the molecular mechanism underlying the cellular action of this class of anti-inflammatory compounds.

INTRODUCTION

The active compounds from willow (*Salix alba* L.) barks, salicylic acid (SA) or salicylates, have been used to treat pain and fever since prehistoric times (Lichterman, 2004; Yin et al., 1998). Based on the structure of SA, various derivatives have been developed as novel non-steroidal anti-inflammatory drugs (NSAIDs; Figures 1A and S1B), such as aspirin (acetylsalicylic acid, ASA) and ibuprofen (IBP) (Yin et al., 1998). NSAIDs, including SA, have been well documented as targeting the prostaglandin biosynthesis enzyme cyclooxygenase-2 (COX-2), thus suppressing the inflammatory response in mammalian cells (Duggan et al., 2011; Kurumbail et al., 1996; Lichterman, 2004; Selinsky et al., 2001; Yin et al., 1998).

In plants themselves, SA is a stress signal, and it is perceived by the NON-TRANSCRIPTION OF PATHOGENESIS-RELATED GENES (NPR) receptors to regulate plant immunity (Ding et al., 2018; Durrant and Dong, 2004; Fu et al., 2012; Wu et al., 2012). Meanwhile, SA can also function through various SA binding proteins (Choi et al., 2015, 2016; Klessig et al., 2016), and SA participates in regulating plant growth and development (Kazan and Manners, 2009; Wang et al., 2007). This developmental role of SA is realized via crosstalk with the transport mechanism for the phytohormone auxin (Du et al., 2013; Pasternak et al., 2019; Rong et al., 2016; Wang et al., 2017). SA regulates root development through both the clathrin-mediated endocytosis pathway (Du et al., 2013; Wang et al., 2016) and protein phosphatase 2A (PP2A)-mediated (de)phosphorylation of PIN-FORMED (PIN) auxin transporters (Tan et al., 2020a), together regulating the plasma membrane (PM) targeting and polar distribution of PINs (Grones and Friml, 2015). Via this mechanism, SA regulates PIN-mediated directional auxin fluxes and auxin transport-mediated development. However, little is known about the effects of NSAIDs in plants—whether they preserve the function of SA or even have any activity at all.

Plant growth and development require the rigorous spatial-temporary distribution of the phytohormone auxin, which depends on both efflux and influx transporters (Adamowski and Friml, 2015; Armengot et al., 2016; Luschnig and Vert, 2014). Throughout the auxin research, synthetic auxin transport

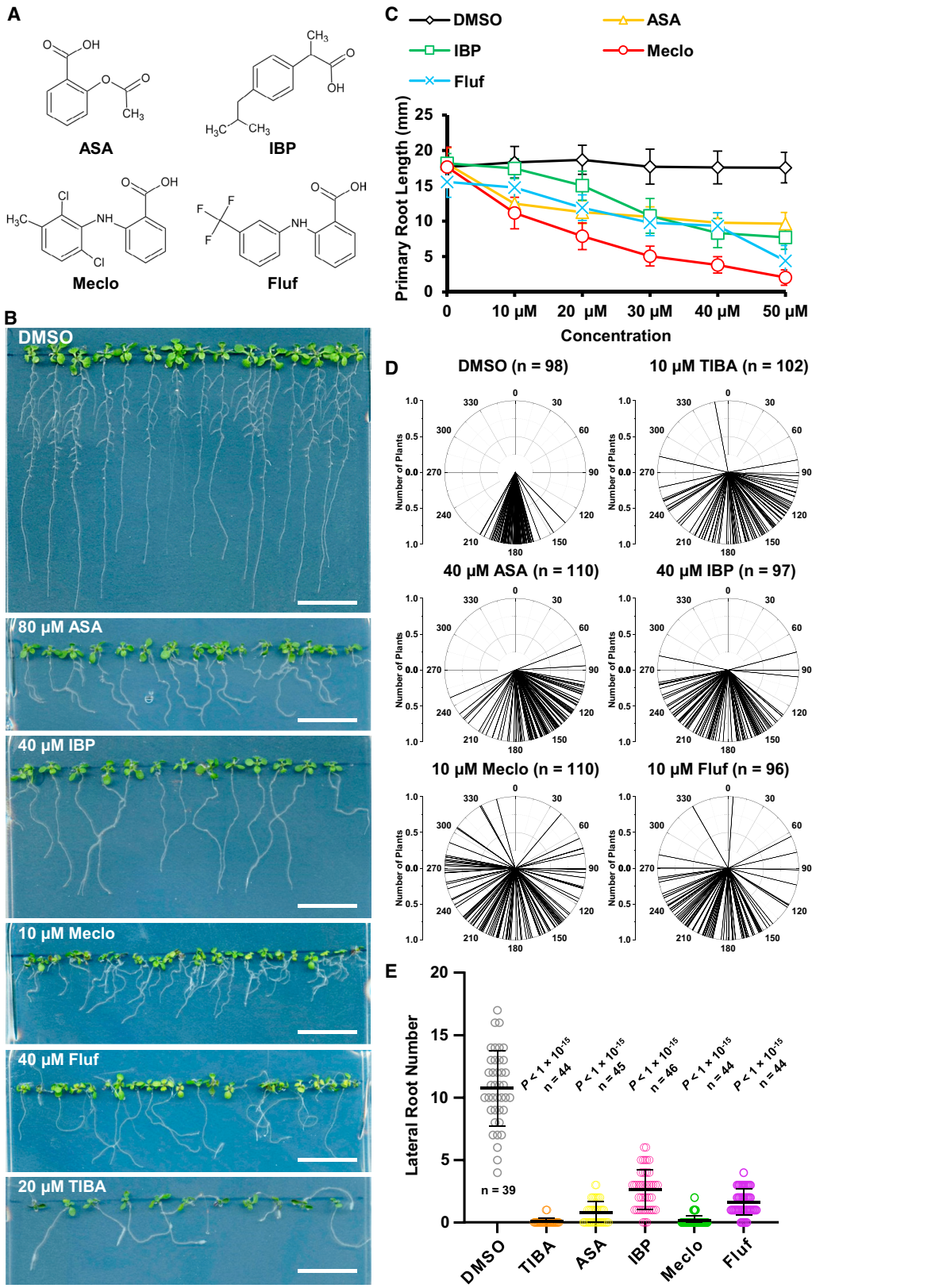

(legend on next page)

inhibitors (ATIs; Figure S1A) and auxin analogs (e.g., 1-naphthaleneacetic acid [NAA], 2,4-D) have played crucial roles in the characterization of molecular components in the auxin pathway, including its biosynthesis, transport, and signaling (Garbers et al., 1996; Ruegger et al., 1997). Using the ATIs 1-*N*-naphthylphthalamic acid (NPA) and 2-carboxyphenyl-3-phenylpropane-1,2-dione (CPD) as selection stress, the *transport inhibitor response* (*tir*) mutants were identified (Mockaitis and Estelle, 2008; Peer, 2013; Ruegger et al., 1998). TIR1 and its close homologs AUXIN SIGNALING F-BOXs (AFBs) were later established as nuclear auxin receptors regulating the expression of downstream genes (Kieffer et al., 2010; Salehin et al., 2015) and non-transcriptional root growth (Fendrych et al., 2018; Gallei et al., 2020). Moreover, PP2AA1 (also known as ROOTS CURL ON NPA1 [RCN1]) was identified from a forward genetic screen for NPA hypersensitive mutant, and has been found to be an essential regulator of PIN auxin transporters (Garbers et al., 1996; Michniewicz et al., 2007; Tan et al., 2020a). Subclasses of ATIs such as 2,3,5-triiodobenzoic acid (TIBA) and 2-(1-pyrenoyl) benzoic acid (PBA) interfere with the dynamics of the actin cytoskeleton and thus the related endocytosis and endocytic trafficking processes involved in PIN delivery (Dhonukshe et al., 2008; Geldner et al., 2001; Zhu et al., 2016).

Here, we uncover the striking activity of NSAIDs in shaping root morphology, in a manner similar to ATIs. Cell biology and biochemical investigation have revealed that NSAIDs, via targeting the immunophilin-like protein TWISTED DWARF1 (TWD1, also called FKBP42), participate in regulating actin cytoskeleton dynamics and thus endomembrane trafficking processes. These affect the trafficking of numerous PM-resident proteins, including PIN auxin transporters. Our discoveries provide insights into the molecular mechanism of NSAIDs in various organisms.

RESULTS

Triple Inhibitory Effects of NSAIDs on *Arabidopsis* Root Morphology

Given the fact that both SA and synthetic NSAIDs function in a common way (i.e., targeting the COX-2 enzyme to inhibit the prostaglandin biosynthesis and ultimately the inflammatory response in mammalian cells) (Duggan et al., 2011; Yin et al., 1998), we were wondering whether these synthetic NSAIDs could retain some SA bioactivity in plants. To address this question, we grew *Arabidopsis* seedlings on plates with different concentrations of NSAIDs and found that most of them exhibited a pronounced effect in the 10- to 100-μM range. Notably, seedlings grown on NSAIDs (80 μM ASA, 40 μM IBP, 10 μM meclofenamic acid [Meclo], and 40 μM flufenamic acid [Fluf], respectively, given different activities) exhibited shorter and agravitropic primary roots (Figures 1B–1D, S1C, and S1D) and fewer or no lateral roots than those on the DMSO or 3-OH-BA controls (Figures 1B, 1E, and S1C). These specific "triple inhibition" physiological effects are highly related to auxin, which is essential for (1) primary root elongation, revealed by the *monopteros/auxin response factor5* (*mp/arf5*) mutant, although higher concentrations of auxin suppress root elongation (Fendrych et al., 2018; Hardtke and Berleth, 1998); (2) lateral root formation, revealed by *solitary root* (*slr*), *arf7 arf19*, *pin1*, *pin3*, and *aux1 lax3* (Benková et al., 2003; Chen et al., 2015; Harper et al., 2000; Swarup et al., 2008; Wang et al., 2015); and (3) root gravitropism, revealed by *auxin resistant3* (*axr3*), *arf10 arf16*, *pin2*, and *auxin1* (*aux1*) (Luschnig et al., 1998; Marchant et al., 1999; Rouse et al., 1998; Wang et al., 2005). In addition, seedlings exhibit similar triple inhibition response under chemical treatment with ATIs, such as NPA and TIBA, as reported previously (Ruegger et al., 1997) and also shown here for TIBA as positive controls (Figures 1B, 1D, 1E, S1C, and S1D). These observations indicate that NSAIDs, similar to TIBA, cause strong triple inhibition physiological effects, probably through compromising the auxin function *in planta*.

NSAIDs Compromise Asymmetric Auxin Distribution and Patterning in Root Meristem

To further test the effect of NSAIDs in the auxin pathway, we used the *DR5rev::GFP* auxin reporter (Friml et al., 2003). *DR5rev::GFP* seedlings were grown constantly on plates with different compounds (40 μM ASA, 40 μM IBP, 40 μM Meclo, 40 μM Fluf, 10 μM TIBA, or DMSO as the solvent control), and NSAIDs caused an over-proliferation of cells expressing *DR5rev::GFP*, similar to TIBA (Figures 2A and S2A). The auxin maxima are essential for the distal differentiation of root columella cells (Ding and Friml, 2010; Friml et al., 2002; Wang et al., 2005), which develop starch-filled amyloplasts (statoliths) as gravity sensors (Friml et al., 2002; Nakamura et al., 2019; Swarup et al., 2005; Wang et al., 2005). Staining with Lugol's solution clearly labeled those statoliths in columella cells under DMSO treatment, whereas TIBA or NSAID treatments led to an expansion of the area (Figures 2B and S2B), correlated with the *DR5* pattern. With a newly developed, more sensitive auxin responsive reporter, *DR5v2::tdTomato;DR5rev::n3GFP* (Liao et al., 2015), it was clearly shown that there was an increase at the lower side of the lateral root cap under a gravi-stimulus by 90° reorientation (Figures 2C and 2D). By contrast, NSAIDs or TIBA could block this asymmetric *DR5* re-distribution (Figures 2C and 2D), suggesting a similar action mode for both known

Figure 1. NSAID Treatments Lead to Triple Inhibitory Response for *Arabidopsis* Roots Morphologically

(A) Chemical structures of representative NSAIDs, illustrated using the ChemSketch program.

(B) Representative images showing the morphological changes of 10-day-old Col-0 seedlings grown on MS media supplemented with NSAIDs at indicated concentrations. Scale bars, 2 cm.

(C) Dose-dependent effect of NSAIDs inhibiting primary root elongation. Seven-day-old Col-0 seedlings; n = 60. DMSO is the solvent control.

(D) NSAIDs interfered with root gravitropism. Seven-day-old Col-0 seedlings grown constantly on MS medium supplemented with DMSO, TIBA, or NSAIDs, as indicated. Each line represents the root tip angle of 1 individual seedling in polar bar charts.

(E) NSAIDs suppressed lateral root formation. The emerged lateral roots of 10-day-old Col-0 seedlings treated with NSAIDs were counted; n = 39, 44, 45, 46, 44, and 44 seedlings, respectively. p values were calculated by comparing different treatments to DMSO with an unpaired t test with Welch's correction.

See also Figure S1.

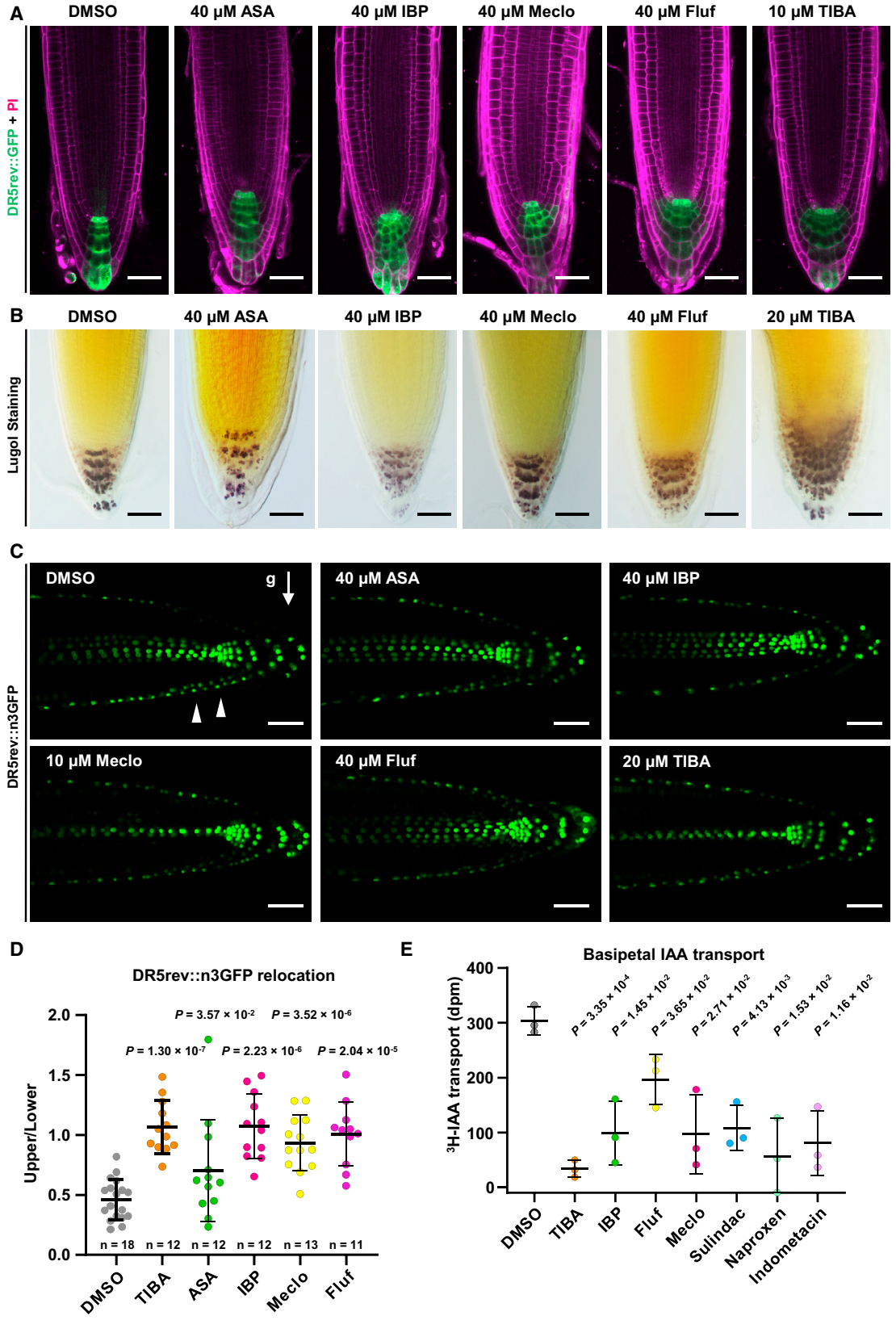

(legend on next page)

ATIs and NSAIDs on the shootward (basipetal) auxin transport and thus gravitropism.

Next, we used the tobacco BY-2 (*Nicotiana tabacum* L. cv. Bright Yellow-2) cell system (Petrášek et al., 2006) to study the effect of NSAIDs on auxin transport directly. NAA is a lipophilic synthetic auxin analog, which shows auxin activity similar to that of the natural indole 3-acetic acid (IAA) but does not require the AUX1 auxin influx carrier (importer) to enter into cells. The transport assay with [^{3}H]-NAA in BY-2 cells showed that 40 μM Meclo, 40 μM Fluf, 40 μM IBP, or 40 μM flurbiprofen (Flur) enhanced the initial accumulation of [^{3}H]-NAA with the quick formation of a plateau that corresponds to the formation of equilibrium between the influx and efflux (Figures S2C and S2D). Moreover, treatment with NSAIDs led to kinetics of [^{3}H]-NAA retention that are similar to the previously described SA (Figure S2D; Tan et al., 2020a). This suggests an inhibitory effect of NSAIDs on auxin efflux, possibly through interfering with subcellular trafficking of the efflux carriers similar to SA, or through the participation of NSAIDs in NAA metabolism in BY-2 cells (Hošek et al., 2012). The application of TIBA led to a continuous increase in [^{3}H]-NAA accumulation (Figure S2C), which indicates that it has a different mode of action in BY-2 cells. To test the effect of NSAIDs on auxin transport *in planta*, we further measured the rootward (basipetal) auxin transport with [^{3}H]-IAA in etiolated *Arabidopsis* hypocotyls. With [^{3}H]-IAA and NSAIDs dissolved in agarose droplets, there was a significant decrease in auxin transport under NSAIDs treatment (Figure 2E). Collectively, these results suggested that NSAIDs could specifically suppress auxin efflux.

NSAID Treatment Inhibits Endocytosis and Endosomal Trafficking

Auxin efflux is facilitated by two different families of exporters, the PIN efflux carriers and a subset of ABCB (PGP) transporters (Adamowski and Friml, 2015; Geisler et al., 2005; Luschnig and Vert, 2014; Petrášek et al., 2006). There are multilevel regulations of auxin exporters, at both transcriptional (Chen et al., 2015; Wang et al., 2015) and post-translational levels (Armengot et al., 2016); the polar localization of PINs is highly dependent on the endomembrane system, across secretion, endocytosis, and endocytic trafficking (Adamowski and Friml, 2015; Glanc et al., 2018). This can be revealed by the effect of brefeldin A (BFA) or BFA agonists/antagonists on PIN/ABCB recycling, auxin transport, and morphological response (Geldner et al., 2003; Kania et al., 2018; Kleine-Vehn et al., 2009; Mishev et al., 2018), as well as genetic tools compromising the endocytosis or the endocytic trafficking pathway, such as *XVE>>AUXILIN-LIKEs* (Adamowski et al., 2018; Glanc et al., 2018), *gnom^{R5}* (Geldner et al., 2003; Kleine-Vehn et al., 2008), or *ala3 (aminophospholipid atpase3)* lines (Zhang et al., 2020). BFA is a widely used inhibitor for ARF-guanine nucleotide exchange factors (GEFs) that regulates trafficking throughout secretion, endocytic trafficking, and recycling (Geldner et al., 2003; Naramoto et al., 2014; Richter et al., 2014; Tanaka et al., 2009). Constant BFA treatment, via abolishing the recycling, switches basal-localized PINs to the apical side (Kleine-Vehn et al., 2009). Nonetheless, BFA abolishes PIN2 polarity establishment in *big3*, in the background of which it mainly blocked secretion, suggesting both endocytosed and newly synthesized pathways are required for PIN2 polarity (Glanc et al., 2018). One subset of ATIs, including NPA and TIBA, specifically inhibit auxin export (Petrášek et al., 2003; Teale and Palme, 2018). One mechanism was proposed in which they interfere with the cytoskeleton to regulate the endomembrane trafficking pathway, thus modulating the subcellular localization of PIN and ABCB transporters, among many others (Dhonukshe et al., 2008; Geldner et al., 2001; Zhu et al., 2016; Zou et al., 2019).

Our previous studies suggested that SA may interfere with the clathrin-mediated endocytosis pathway to compromise PIN trafficking and also inhibit PP2A activity to affect PIN subcellular localization (Du et al., 2013; Tan et al., 2020a). To test whether NSAIDs modulate the subcellular localization of PIN proteins, we grew *PIN2::PIN2-GFP;VHA-a1* (Vacuolar H$^+$-ATPase subunit a1)*::VHA-a1-mRFP* (monomeric red fluorescent protein) seedlings constantly on plates supplemented with NSAIDs or TIBA (as control). The results showed that the apical polarity of PIN2-GFP in epidermal cells decreased following treatments with NSAIDs (Figures 3A and 3B). As mentioned above, PIN2 cycles between PM and the endomembrane pool, and BFA treatments lead to the internalization of PIN2 protein in a large stack of the endomembrane compartments, co-localized with VHA-a1-mRFP, the so-called BFA body (Geldner et al., 2001; Narasimhan et al., 2020). Furthermore, NSAIDs could compromise the BFA compartmentation of both PIN2-GFP and VHA-a1-mRFP (Figures 3C and 3D), suggesting defects in the underlying endocytosis or endomembrane trafficking process. These inhibitory effects may explain the polarity changes that occur under long-term NSAID treatments. In line with the observation that NSAIDs interfered with the BFA compartmentation of EEs/TGN (early endosomes/*trans*-Golgi network), there were also defects

Figure 2. NSAID Treatments Interfere with Auxin Responses in *Arabidopsis* Roots

(A) The regular auxin-responsive pattern of DR5rev::GFP was disrupted by NSAID treatments. Five-day-old *DR5rev::GFP* seedlings grown on plates containing NSAIDs with indicated concentrations were stained with propidium iodide (PI) and imaged with confocal laser scanning microscopy (CLSM), respectively, 20×; n = 10–12, and scale bars, 20 μm.

(B) Constant NSAID treatments changed the pattern of statocytes. Five-day-old Col-0 seedlings under indicated treatments were stained with Lugol's solution and then imaged with a differential interference contrast (DIC) microscope, 40×; n = 15–20, and scale bars, 20 μm.

(C and D) NSAID treatments suppressed the re-distribution of DR5rev::n3GFP pattern under gravi-stimulation. Five-day-old *DR5v2::ntdTomato; DR5rev::n3GFP* seedlings grown on normal plates were transferred to DMSO/NSAID/TIBA-containing plates, and turned by 90°. Root tips were imaged with CLSM for the GFP channel, 20×. (C) Representative images. Scale bars, 20 μm. (D) The upper:lower ratio for the DR5 signal was measured to indicate the relocation; n = 18, 12, 12, 12, 13, and 11, respectively. p values were calculated by comparing different treatments to the DMSO control with an unpaired t test with Welch's correction.

(E) NSAIDs inhibited basipetal (rootward) auxin transport in hypocotyls of *Arabidopsis* etiolated seedlings. Fifteen seedlings were pooled together as 1 biological replicate for measurement; n = 3. p values were calculated by an unpaired t test with Welch's correction.

See also Figure S2.

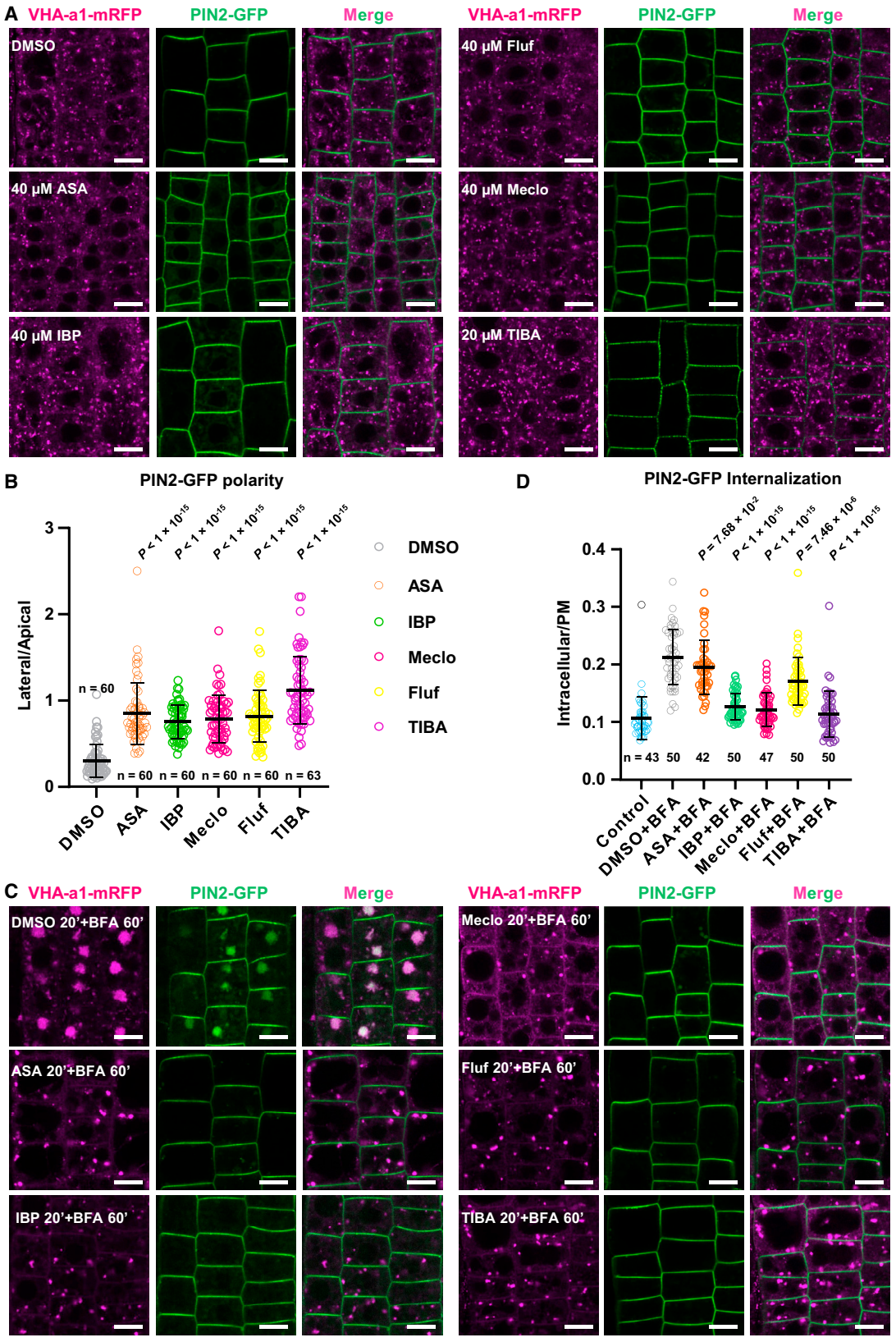

(legend on next page)

in the trafficking or recycling of other PM-resident cargo proteins, including ABCB19-GFP, ABCB1-GFP, and plasma membrane intrinsic protein 2a (PIP2a)-GFP (Figure S3A). This suggests that the effects of NSAIDs are not specific to PIN proteins. Furthermore, BFA washout released both PIN2-GFP and VHA-a1-mRFP from the BFA bodies also in the presence of NSAIDs, indicating that the physiological effects of NSAIDs are reversible (Figures S3B–S3E). Notably, the NSAID treatments led to the aggregation of PIN2-GFP and EEs in certain endomembrane structures, which are larger than the EEs/TGN, but smaller than BFA bodies (Figures 3C, S2E, and S3B–S3E). This is similar to the effects of reported compounds acting on the actin cytoskeleton, including actin filament-stabilizing drugs Jasplakinolide (Jasp) and TIBA, as well as the actin filament (AF)-depolymerizing chemical latrunculin B (LatB) (Figure S2E; Narasimhan et al., 2020). To further test the specific effect of NSAIDs on endocytosis, we tested whether NSAIDs could affect the uptake of a lipophilic fluorescent dye, FM4-64. With the same concentrations, NSAIDs could block FM4-64 uptake (Figures 4A and 4B). These observations reveal a dual function of NSAIDs in both endocytosis and endomembrane trafficking, and NSAIDs impair the BFA compartmentation of PM-resident cargo proteins possibly via perturbation of the endomembrane system.

NSAIDs Cause Aggregation of Multiple Endomembrane Compartments via Suppressing Endosomal Mobility

Next, to test whether NSAIDs affect endosomal morphology or distribution, we examined the subcellular localization of a set of endomembrane makers, including ADP-ribosylation factor 1 (ARF1)-GFP, clathrin light chain 2 (CLC2)-GFP, GNOM-GFP, GNOM-like 1 (GNL1)-YFP, and VHA-a1-GFP (Figures 4C and S4). In line with the suppression of FM4-64 uptake and the aggregation of FM4-64 labeled endosomes upon treatments with NSAIDs or TIBA, those markers exhibited similar aggregations, suggesting a common regulatory mechanism. Notably, it was observed for the late endosome marker ARA7 (*Arabidopsis thaliana* homologous to the mammalian *ras* gene 7, also known as *Arabidopsis* Rab GTPase Homolog F2b [RabF2b])-YFP (Figures 4D and S4B). These observations suggest that NSAIDs may interfere with vesicle trafficking via a common machinery involved in the regulation of the entire endomembrane system.

The aggregation of endosome markers may be due to their lower mobility under NSAID treatment. Further live imaging by confocal laser-scanning microscopy (CLSM) with an early endosome marker, VHA-a1-GFP, revealed that NSAID treatments led to the aggregation of endosomes, the dynamics of which slowed down upon treatment with Meclo or Fluf, in comparison to the DMSO control (Figures 5A and 5B; Video S1). Experiments with more NSAIDs obtained similar results, further confirming their inhibitory effects on endosomal mobility (Figure S5A; Video S2). Interestingly, the effective concentrations for different NSAIDs are distinct, which is in line with their different physiological activity on root morphology. A similar aggregation was also observed for TIBA (Figure S5A; Video S2), suggesting a potential common mechanism.

Our observations reveal that NSAIDs interfere with the mobility of various types of endosomes without selectivity, suggesting a common regulatory mechanism. We hypothesize that NSAIDs may act through the cytoskeleton, microtubules (MTs) and AFs, which are highways for vesicle trafficking (Geldner et al., 2001; Narasimhan et al., 2020). We first tested the effect of NSAIDs on the dynamics of actin cytoskeleton with a *35S::GFP-Fimbrin* AF marker (Wang et al., 2004) by live imaging. Following treatments with Meclo or Fluf, the mobility of the actin cytoskeleton was largely suppressed compared with the DMSO control (Figure 5C). Likewise, treatments with other NSAIDs or TIBA led to a similar arrest of AF dynamics (Figure S5B). Qualitatively, the effect of Meclo and Fluf on AF dynamics is different from that of those well-established drugs acting directly on AFs, such as Jasp and LatB, which led to dysfunctional fragmented AFs (Figure S5C). By quantifying the skewness, all of these compounds caused the thickening of AFs (Figure S5D). We hypothesized that this effect of Meclo and Fluf may be due to their inhibitory action on AF dynamics, whereas Jasp and LatB interfere with the AF organization directly. Furthermore, co-treatments by Jasp or LatB with Meclo or Fluf did not significantly differ from the Jasp and LatB treatments alone (Figures S5C and S5D), suggesting that Meclo and Fluf function via certain targets indirectly modulating AF dynamics and function. Our results suggest that NSAIDs inhibit endomembrane trafficking through hindering actin cytoskeleton dynamics.

NSAIDs Function through TWD1

These above observations suggest that the action mode of NSAIDs is similar to that of TIBA. At low concentrations (1–10 μM), TIBA exhibits a pronounced inhibitory effect on auxin export similar to another well-known ATI, NPA, whereas at high concentrations (10–50 μM), both TIBA and NPA suppress the endocytic trafficking process and the subsequent PM targeting of multiple cargo proteins, including PIN auxin carriers (Dhonukshe et al., 2008; Geldner et al., 2001; Ruegger et al., 1997; Zhu et al., 2016; Zou et al., 2019). It has been shown that NPA and other

Figure 3. NSAID Treatments Impair PIN2 Polarity and Trafficking

(A and B) NSAID treatments impaired the polar distribution of PIN2-GFP in root epidermal cells. Five-day-old *pPIN2::PIN2-GFP; pVHA-a1::VHA-a1-mRFP* seedlings were treated with DMSO, 40 μM ASA, 40 μM IBP, 40 μM Meclo, 40 μM Fluf, or 20 μM TIBA for 30 min, and then were co-treated with 37.5 μM BFA for 60 min before imaging with CLSM. (A) Representative images, 63× oil objective lens; n > 10, and scale bars, 10 μm. (B) Quantification of the lateral:PM fluorescence ratio of PIN2-GFP by Fiji; n = 60, 60, 60, 60, 60, and 63 cells, respectively.

(C and D) NSAIDs inhibited the BFA body formation of both PIN2-GFP and VHA-a1-mRFP in root epidermal cells. Five-day-old *pPIN2::PIN2-GFP; pVHA-a1::VHA-a1-mRFP* seedlings were treated with DMSO, 40 μM ASA, 40 μM IBP, 40 μM Meclo, 10 μM Fluf, or 20 μM TIBA for 30 min, and then were co-treated with 37.5 μM BFA for 60 min before imaging with CLSM. (C) Representative images, 63× oil objective lens, n > 10, and scale bars, 10 μm. (D) Quantification of the fluorescence intracellular:PM ratio of PIN2-GFP by Fiji; n = 43, 50, 42, 50, 47, 50, and 50, respectively.

p values were calculated by comparing different treatments to the DMSO control (B) or "DMSO+BFA" group (D) with an unpaired t test with Welch's correction. See also Figures S2 and S3.

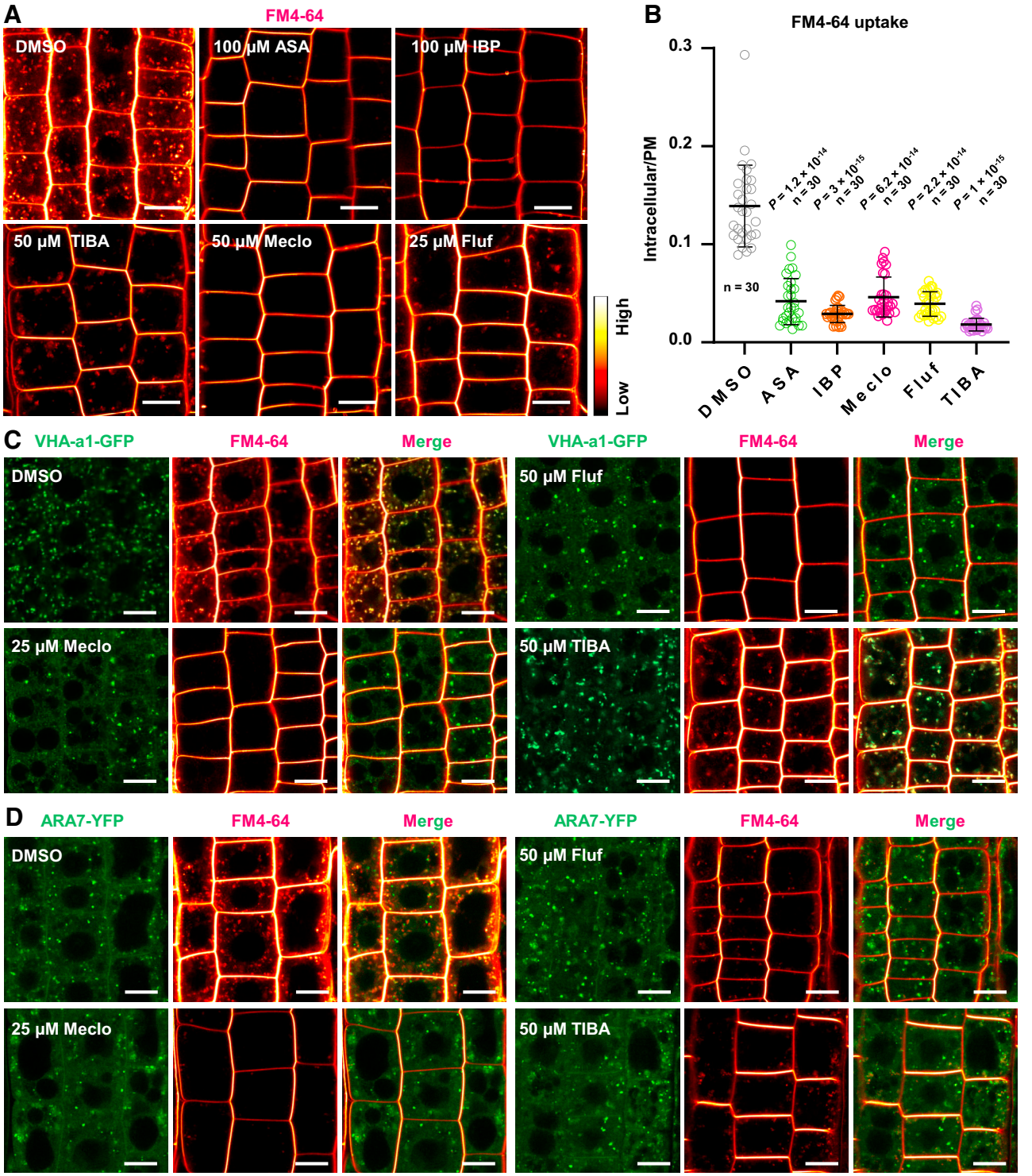

Figure 4. NSAIDs Inhibit Endocytosis and Lead to Endosomal Aggregation

(A and B) NSAID treatments inhibited the uptake of FM4-64. Five-day-old Col-0 seedlings were treated with DMSO, 50 μM Meclo, 25 μM Fluf, or 50 μM TIBA for 15 min, and added with 2 μM FM4-64 in the same system for further staining 15 min before imaging with CLSM. (A) n = 7–13, representative photos were shown. Scale bars, 10 μm. (B) Quantification of the fluorescence intensity ratio of the intracellular:PM signal; n = 30 cells for each. p values were calculated by comparing different treatments to the "DMSO+BFA" group with an unpaired t test with Welch's correction.

(legend continued on next page)

ATIs regulate the actin cytoskeleton via binding to TWD1/FKBP42, which is an immunophilin protein functioning as a chaperone of ABCB transporters and also a regulator of actin cytoskeleton via ACTIN7 (ACT7) (Geisler and Bailly, 2007; Wang et al., 2013; Zhu et al., 2016). A recent study revealed that TIBA also binds to the actin-related protein VILLIN4 (Zou et al., 2019). These findings suggest that the actin cytoskeleton and actin-dependent vesicle trafficking processes are additional targets of ATIs. Given the similar physiological and cell biological effects of NSAIDs and ATIs, we hypothesized that they may act via the same pathway.

To test this, we examined the sensitivity of *twd1-3* and *act7-4* mutants (Geisler et al., 2003; Gilliland et al., 2003; Zhu et al., 2016) to NSAIDs that exhibited no further effects to the agravitropic root growth of *twd1-1* or *act7-4* (Figures S5E–S5G). A similar response was reported for the growth of *twd1-1* and *act7-4* on ATIs (Zhu et al., 2016), suggesting a common mechanism. Further experiments with the *DR5rev::GFP* reporter, to monitor shootward polar auxin transport during the root gravitropic response, failed to detect any further decrease in DR5 relocation in *twd1-3*, which is consistent with Meclo's and Fluf's interfering with polar auxin transport via TWD1 (Figures 6A and 6B). Moreover, the inhibition of BFA-induced aggregation of PIN2-GFP and VHA-a1-mRFP by Meclo and Fluf was partially suppressed by the *twd1-3* mutation, further confirming that impairing endosomal mobility by these two compounds requires at least partly TWD1 function (Figure S6A). Next, we tested the role of ACT7 in endosomal mobility with the *act7-4 SYP61::SYP61-CFP* EE/TGN reporter (Zhu et al., 2016), and results showed that there is certain constitutive aggregation of SYP61-CFP, which is similar to, although not as strong as, the effects of Meclo and Fluf. Additional treatments with these two compounds did not increase the aggregation to the same degree as that in wild-type (WT) background, suggesting an involvement of ACT7 in the process (Figure S6B). Moreover, when growing constantly on solid Murashige and Skoog (MS) media with IBP or other NSAIDs, both Col-0 and *35S::MAP4-GFP* (WT) seedlings exhibited a twisted growth manner (Figures 6C, S6C, and S6D) that is similar to the *twd1-3* and *act7-4* mutants (Figures 6D and 6E). Interestingly, a high concentration (40 μM) of Fluf also inhibited root hair formation, which was not observed in the *twd1-3* or *act7-4* mutants, however (Figures 6D, 6E S6C, and S6D). Although the actin cytoskeleton was reported to be involved in multiple processes during root hair formation, the underlying mechanism for Fluf regulating root hairs requires further investigation. Given that both *twd1-3* and *act7-4* mutants exhibit strong defects in root gravitropism and root morphology, we cannot exclude the possibility that additional targets may exist for Meclo and Fluf.

Neither NSAID treatments nor the *twd1* mutation had an obvious effect on MAP4-GFP signal distribution (Figures S6D and S6E), implying that NSAIDs or TWD1 function independently of MTs. Further analysis with the AF marker GFP-fABD2 revealed that AF organization was less sensitive to Meclo/Fluf in *twd1-3* or *act7-4* than in WT in AF skewness (Figures 6F and 6G). To conclude, NSAIDs may function via a TWD1-ACT7-AF pathway, repressing endosomal mobility. In line with the notion that NSAIDs may target multiple proteins in distinct pathways, the *twd1-1* mutant is hypersensitive to NSAIDs in terms of AF stability in the division zone (Figure S7A), suggesting the presence of other TWD1-independent regulatory modes.

NSAIDs Bind Directly to the FK506-Binding Protein (FKBP) Domain (FKBD) of TWD1 and Inhibits Its Chaperone Activity

In silico protein-ligand docking analysis revealed that most NSAIDs have the potential to bind to the FKBD of TWD1 (Table S1; Zhu et al., 2016). Notably, those drugs exhibiting higher physiological activity, such as Fluf and Meclo, were also predicted to be good candidates for TWD1 binding, with calculated dissociation constants (K_D) of 61.5 and 159.6 μM (fixed docking; Table S1).

With pure recombinant protein for the TWD1 FKBD protein, we performed surface plasmon resonance (SPR) experiments to measure the binding affinities of NSAIDs to it. The results revealed that both Meclo and Fluf directly bound to the TWD1 FKBD, with kinetic K_D of 51.0 ± 6.1 μM and 172.5 ± 19.1 μM, respectively (Figures 7A, 7B, S7B, S8A, and S8B), which are in remarkable agreement with *in silico* calculated ones (Table S1). Further SPR assays with NSAID compounds revealed that only a subset of those (Meclo, Fluf, mefenamic acid, diclofenac, indomethacin, and difusinal) showed a detectable binding to the TWD1 FKBD, but not others (Figure S7B). These results indicate that the NSAID compounds exhibit differential binding affinity toward the TWD1 FKBD, although they show similar bioactivity in plants. We speculate that those compounds showing lower activity, such as IBP, may have lower binding affinity to TWD1 and thus escape detection by SPR. However, it cannot be excluded that other non-TWD1 targeting NSAIDs may function via other protein targets, and this awaits further characterization.

Given the chaperone activity of TWD1 (Wang et al., 2013; Wu et al., 2010), we further tested the thermostability of citrate synthase, a common substrate of FKBP chaperones (Kamphausen et al., 2002), with or without TWD1 under different concentrations of Meclo, and found that 50 μM Meclo exhibited an inhibitory effect on TWD1 chaperone (holdase) activity, shifting the half-maximal effective concentration (EC_{50}) of TWD1 protein from 81.5 nM (solvent, R^2 = 0.977) to 125.8 nM (R^2 = 0.987). This further supports the direct binding of Meclo to TWD1 and provides evidence that NSAIDs interfere with the activity of TWD1 (Figures 7C and S8C). Meclo targets TWD1 to modulate auxin transport-mediated plant morphogenesis and gravitropism.

(C) NSAID treatments led to aggregation of VHA-a1-GFP-probed EEs/TGN compartments and suppression of FM4-64 uptake in root epidermal cells. Five-day-old *pVHA-a1::VHA-a1-GFP* seedlings were treated with DMSO, 50 μM Meclo, 25 μM Fluf, or 50 μM TIBA for 30 min, and then were co-treated with 2 μM FM4-64 for 15 min before imaging with CLSM, 63× oil, n > 10, and scale bars, 10 μm.

(D) NSAID treatments led to aggregation of ARA7-YFP-probed late endosomes and suppression of FM4-64 uptake in root epidermal cells. Five-day-old *pUBQ10::ARA7-YFP* seedlings were treated with DMSO, 50 μM Meclo, 25 μM Fluf, or 50 μM TIBA for 30 min, and then were co-treated with 2 μM FM4-64 for 15 min before imaging with CLSM, 63× oil, n > 10, and scale bars, 10 μm.

See also Figures S4.

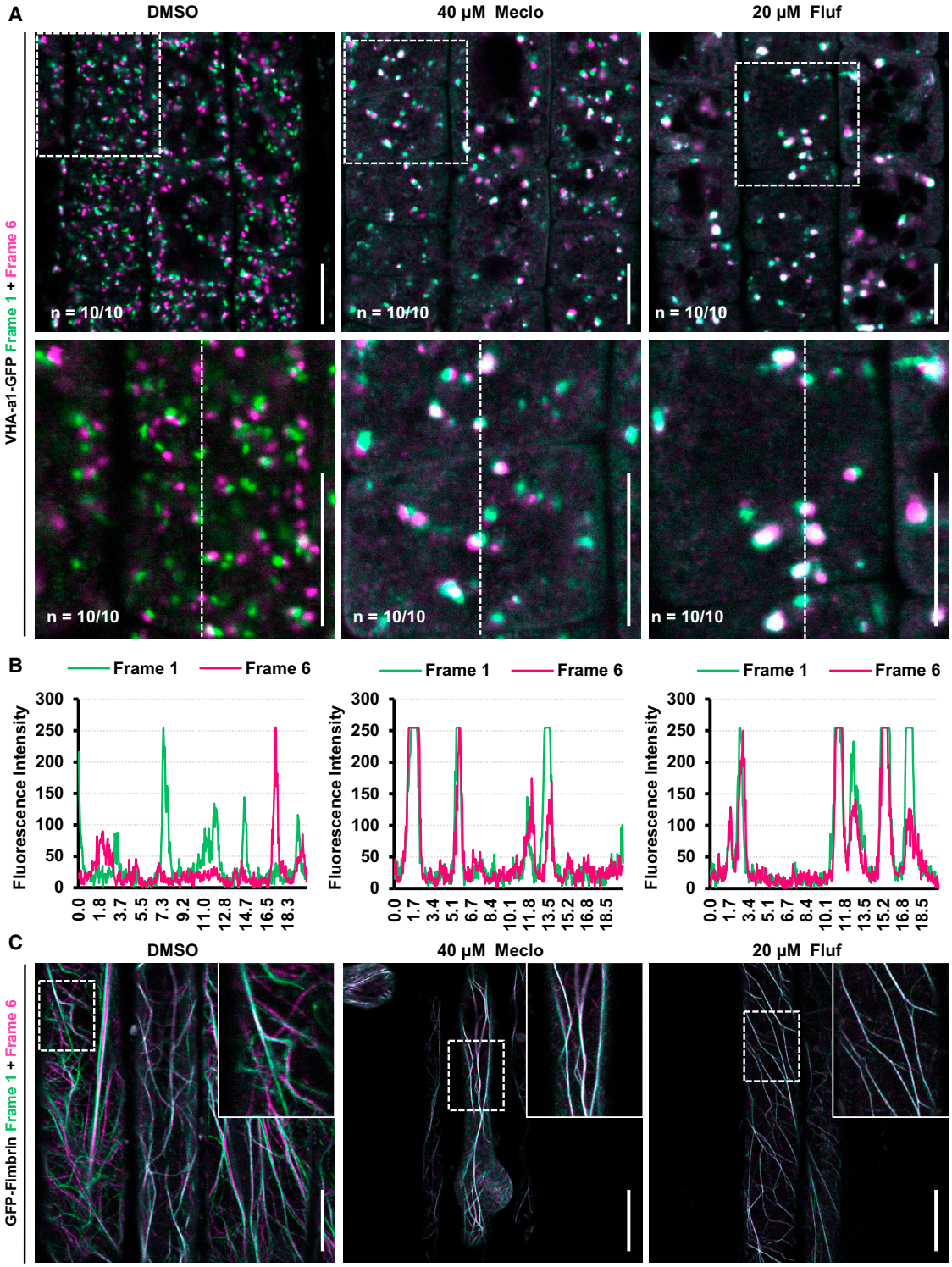

Figure 5. NSAIDs Inhibit the Mobility of EEs and the Dynamics of the Actin Cytoskeleton

(A) Five-day-old *pVHA-a1::VHA-a1-GFP* seedlings were treated with DMSO, 40 μM Meclo, or 20 μM Fluf for 30 min, and then root epidermal cells were imaged with CLSM, 63× oil objective lens. Time-lapse imaging was performed with 5 s/frame, 11 frames, and representative merged image of frame 1 (t = 0, green) and frame 6 (t = 25 s, magenta) were shown; n > 10 and scale bars, 10 μm.

(B) Fluorescence intensity plot indicates that NSAIDs suppressed endosomal mobility with the marker *pVHA-a1::VHA-a1-GFP*.

(legend continued on next page)

To verify whether ATIs and NSAIDs bind to the same surface on the FKBD of TWD1 *in planta*, we tested K79 and H125 mutations in TWD1 previously shown to disrupt NPA binding with transgenic lines *pTWD1::TWD1^{K79I}-CFP* and *pTWD1::TWD1^{H125I}-CFP*. Neither K79I nor H125I mutation abolished the full function of TWD1, although K79I only partially rescued the growth defects of *twd1-3* (Figure S8D). Further physiological tests revealed that K79I and H125I mutation only slightly decreased the plants' sensitivity to Meclo or Fluf (Figures S8E and S8F). Therefore, we used quantum chemical calculations to analyze the potential interactions for NSAIDs and the TWD1 FKBD (Zhu et al., 2016). Unlike NPA, these analyzed NSAIDs seemed not to bind the same sites as NPA (Table S2), except with the occurrence of a drastic conformational change in the protein that generates the action of forces and chemical spaces far beyond the parameters studied. Another possibility is the action of NSAIDs on an additional TWD1 interactor. Collectively, both *in planta* assays and *in silico* quantum chemical calculations suggest that Meclo and Fluf use a distinct site from NPA for binding to TWD1 FKBD, which could also explain the different action modes on the actin cytoskeleton.

DISCUSSION

NSAIDs Target TWD1 to Regulate Actin Cytoskeleton Dynamics and Endomembrane Trafficking

Our studies reveal that NSAIDs, acting similarly to the auxin transport inhibitors such as TIBA at both physiological and cellular levels, interfere with auxin activity by suppressing its polar transport. Moreover, NSAIDs impair the dynamics of the actin cytoskeleton, thereby hampering endosomal mobility. Finally, and most important, many NSAIDs bind directly and inhibit TWD1, a promising FKBP chaperoning a subgroup of auxin-transporting ABCB transporters (Hao et al., 2020; Wang et al., 2013; Xu et al., 2010).

Our data collectively establish a NSAID-TWD1-actin cytoskeleton module, regulating endomembrane dynamics and deliveries of PM proteins, including PIN and ABCB auxin transporters. In this module, NSAID binding to TWD1 would have an inhibitory effect on the actin cytoskeleton, which is indirectly supported by overlapping twisting phenotypes between *twd1-1* or *act7-4* and NSAIDs-treated WT roots. However, given that there are no dramatic changes in PIN subcellular localization in the *twd1* mutant (Bouchard et al., 2006) and that the twisting phenotype caused by NSAIDs in WT is not as strong as in *twd1*, the molecular mechanism underlying NSAID action in plants seems complex. This apparent discrepancy may be explained by a dual effect of NSAIDs on auxin transport and vesicle trafficking, as has been reported for two widely used ATIs, TIBA and NPA. Nonetheless, NPA seems to more specifically inhibit PIN-mediated transport directly, interfering with endomembrane trafficking only at extreme high concentrations; TIBA has a complex mode, with a stronger effect on the latter (Dhonukshe et al., 2008; Dindas et al., 2020; Geldner et al., 2001; Zhu et al., 2016). The auxin transport inhibitor activity of TIBA was first described in the 1940s (Keitt and Baker, 1966; Snyder, 1949). Further chemical and physiological studies of different TIBA analogs revealed that modification at the ortho-position of the benzoic ring is essential for its activity (Keitt and Baker, 1966; Quint and Gray, 2006). Intriguingly, the chemical structures of ATIs and NSAIDs share certain key features (Figures S1A and S1B); i.e., modification at the ortho-position of the benzoic ring seems essential for their bioactivity (Katekar and Geissler, 1977, 1980; Keitt and Baker, 1966; Snyder, 1949). Thus, it would be of interest to study whether some ATIs have anti-inflammatory activity. We cannot exclude the possibility that NSAIDs may regulate the actin cytoskeleton through additional components such as VILLIN proteins (Zou et al., 2019) or by acting on actin itself.

Collective evidence reveals that, despite their common physiological activity as ATIs, NPA and TIBA also exhibit distinct activities and action modes, suggesting distinct molecular targets in plants (Dindas et al., 2020; Geldner et al., 2001; Petrášek et al., 2003; Teale and Palme, 2018; Zhu et al., 2016). We speculate that these synthetic compounds target distinct proteins with different binding affinities, and meanwhile they may be metabolized with variable kinetics, both of which contribute to the complex mode of action at physiological and cellular levels in plants. Notably, unlike NPA, which partially suppressed the twisting phenotype of *twd1* (Wang et al., 2013; Wu et al., 2010), Meclo and Fluf cause twisted roots partly resembling *twd1*. Moreover, the effect of NSAIDs on AF skewness is more likely an indirect effect of their inhibitory effects on AF dynamics. These observations suggest other targets or other modes of action by TWD1 that are due to interaction with non-NPA binding sites. In addition, not all NSAIDs show strong binding to TWD1. Whether this is due to a lower binding affinity or preference for other targets awaits further investigation.

NSAIDs as Potential Chemical Tools in Cell Biology

Our results reveal that NSAIDs interfere with both endocytosis and endocytic trafficking processes. NSAIDs could inhibit the BFA-induced aggregation of endosomes, and NSAID-TWD1 binding for regulating AF dynamics may account for this effect. NSAIDs can also block FM4-64 internalization, indicating a direct effect on the endocytosis process at PM. This strong effect suggests the potential use of NSAIDs as endocytosis inhibitors for plant cell biology. However, given the fact that actin filaments seem not to be involved in clathrin-mediated endocytosis (Narasimhan et al., 2020), this activity is unlikely through the TWD1-AF module. Therefore, the molecular mechanism underlying this bioactivity requires further investigation.

Although synthetic NSAIDs exhibit anti-inflammatory bioactivities similar to those of SA in human cells, little is known about them in the plant system. PATI-2 (2-[4-chloro-3-methylbenzoyl] benzoic acid), an inhibitor of COXs in mammals, was once identified from a large throughput screen for compounds having an

(C) NSAIDs inhibited the dynamics of actin filaments shown with the GFP-fimbrin AF marker. Five-day-old *p35S::GFP-Fimbrin* seedlings were treated with DMSO, 40 μM Meclo, or 20 μM Fluf for 30 min, and then imaging was conducted with CLSM, 63× oil. Time-lapse imaging was performed with 5 s/frame, 11 frames, and representative merged photo of frame 1 (t = 0, green) and frame 6 (t = 25 s, magenta) were shown; n = 10, and scale bars, 10 μm.
See also Figure S5 and Videos S1 and S2.

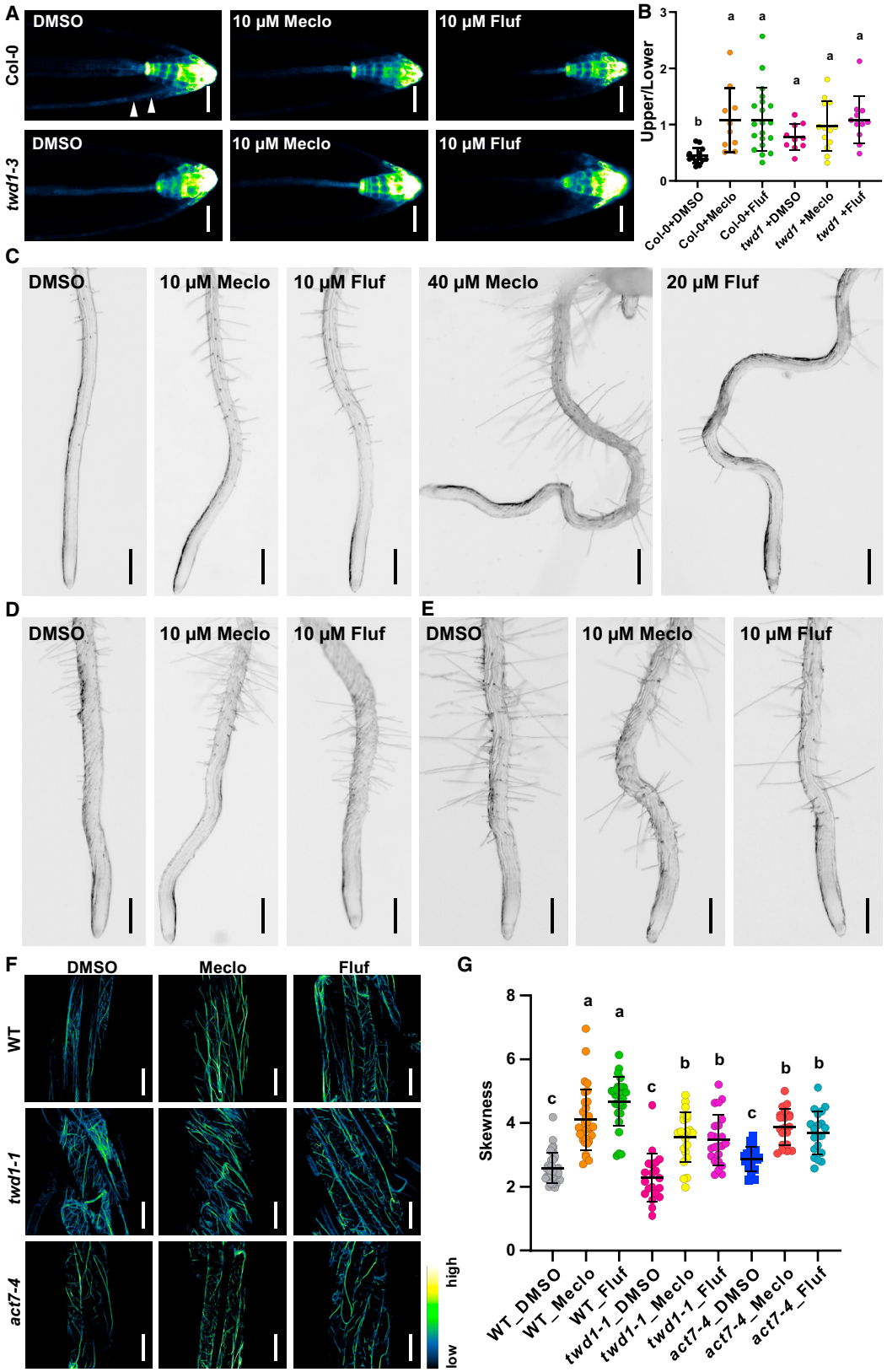

(legend on next page)

impact on leaf vein patterns (Carland et al., 2016), which is highly dependent on directional auxin transport. Notably, PATI-2 exhibits a similar effect as those NSAIDs described in this study on PIN trafficking. It would be of interest to test whether PATI-2 also acts via a TWD1-mediated AF remodeling pathway. In another recent screen for 2,4-Dinduced Ca^{2+} signaling, Fluf came out as one inhibitor, possibly via interfering with the membrane gradients (De Vriese et al., 2019). Given that the *twd1-1* mutant is still responding to NSAIDs and that NSAIDs exhibit differential binding affinities to TWD1 FKBD, we cannot exclude the possibility that these compounds have additional targets.

A Potential Cross-Kingdom-Conserved Mechanism for NSAID-FKBP Function

TWD1/FKBP42 is an immunophilin-like protein, sharing high sequence similarity and domain structure with FKBP38 in humans (Aryal et al., 2015). Notably, FKBP38 is an essential co-chaperone for the trafficking of HERG, a protein related to the long QT syndrome, a cardiac disorder associated with ventricular arrhythmias (Walker et al., 2007). We speculate that NSAIDs may also target FKBP38 to regulate HERG trafficking in mammalian cells. Together with the notions that NSAIDs, including IBP, increase the risk of out-of-hospital cardiac arrest (Mangoni et al., 2010; Sondergaard and Gislason, 2017), it would be of great value to investigate whether the NSAID-FKBP mechanism is conserved and thus is involved in the side effects of NSAIDs on the cardiovascular system.

STAR★METHODS

Detailed methods are provided in the online version of this paper and include the following:

- KEY RESOURCES TABLE
- RESOURCE AVAILABILITY
  - Lead Contact
  - Materials Availability
  - Data and Code Availability
- EXPERIMENTAL MODEL AND SUBJECT DETAILS
  - Plant Materials and Growth Conditions
- METHOD DETAILS
  - Pharmacological Treatments
  - Auxin transport assays in *Arabidopsis* hypocotyls and tobacco BY-2 cells
  - Imaging by confocal laser scanning microscopy (CLSM)
  - FM4-64 uptake assays and PI staining
  - Startolith starch staining with Lugol's solution
  - Image analysis and morphological analysis
  - *In silico* substrate docking analysis and quantum chemical modeling for NSAIDs and TWD1
  - Surface plasmon resonance (SPR) analysis
  - TWD1 chaperone activity assay
  - Accession numbers
- QUANTIFICATION AND STATISTICAL ANALYSIS

SUPPLEMENTAL INFORMATION

Supplemental Information can be found online at https://doi.org/10.1016/j.celrep.2020.108463.

ACKNOWLEDGMENTS

We thank Drs. Sebastian Bednarek (University of Wisconsin-Madison), Niko Geldner (University of Lausanne), and Karin Schumacher (Heidelberg University) for kindly sharing published *Arabidopsis* lines; Dr. Satoshi Naramoto for the *pPIN2::PIN2-GFP; pVHA-a1::VHA-a1-mRFP* reporter; the staff at the Life Science Facility and Bioimaging Facility, Mónika Hrtyan, and Dorota Jaworska at IST Austria for technical support; and Drs. Su Tang (Texas A&M University), Melinda Abas (BOKU), Eva Benková (IST Austria), Christian Luschnig (BOKU), Bartel Vanholme (Gent University), and the Friml group for valuable discussions. The research leading to these findings was funded by the European Union's Horizon 2020 program (ERC grant agreement no. 742985, to J.F.), the People Programme (Marie Curie Actions) of the European Union's Seventh Framework Programme (FP7/2007-2013) under REA grant agreement no. 291734, the Swiss National Funds (31003A_165877, to M.G.), the Ministry of Education, Youth, and Sports of the Czech Republic (project no. CZ.02.1.01/0.0/0.0/16_019/0000738, EU Operational Programme "Research, development and education and Centre for Plant Experimental Biology"), and the EU Operational Programme Prague - Competitiveness (project no. CZ.2.16/3.1.00/21519). S.T. was funded by a European Molecular Biology Organization (EMBO) long-term postdoctoral fellowship (ALTF 723-2015). X.Z. was partly supported by a PhD scholarship from the China Scholarship Council.

AUTHOR CONTRIBUTIONS

S.T. and J.F. conceived and designed the research. S.T., M.D., M. Glanc, X.Z., P.K., and J.L. performed the experiments and analyzed the data. N.F. and A.B.

Figure 6. NSAID Treatment Led to Twisted Growth in Roots, Similar to *twd1-3* and *act7-4* Mutants

(A and B) The *twd1-3* mutation led to decreased shootward auxin transport and abolished the effect of Meclo and Fluf. Five-day-old *DR5rev::GFP* seedlings grown on normal plates were transferred to DMSO/Meclo/Fluf-containing plates, and turned by 90°. Root tips were imaged with CLSM, 20×. (A) Representative images are shown. Scale bars, 20 μm. (B) The upper:lower ratio for the DR5 signal was measured to indicate the relocation; n = 13, 10, 21, 10, 13, and 11, respectively.

(C) NSAID treatments led to twisted root growth. Seven-day-old seedling grown on plates with indicated concentrations of Meclo and Fluf were imaged with a stereomicroscope; n = 20, and scale bars, 100 μm.

(D and E) *twd1-3* (D) and *act7-4* (E) mutants exhibited twisted growth in roots, and Meclo and Fluf treatments did not enhance this further; n = ~10, and scale bars, 100 μm.

(F) z stack showing the AF morphology in *twd1-1* and *act7-4* background under Meclo and Fluf treatments. Five-day-old *35S::GFP-fABD2* seedlings were treated with DMSO, 40 μM Meclo, and 10 μM Fluf, respectively, and subjected to imaging with CLSM; 40× objective; n = 10, and scale bars, 10 μm.

(G) Quantification of the AF skewness under Meclo and Fluf treatments. The same set of samples as in (F) were imaged with CLSM, and the skewness was quantified with Fiji; n = 20.

p values were calculated by comparing different treatments with 1-way ANOVA with Welch's correction, and different letters represent significant difference, $p < 0.05$ (B and G).

See also Figures S6 and S7.

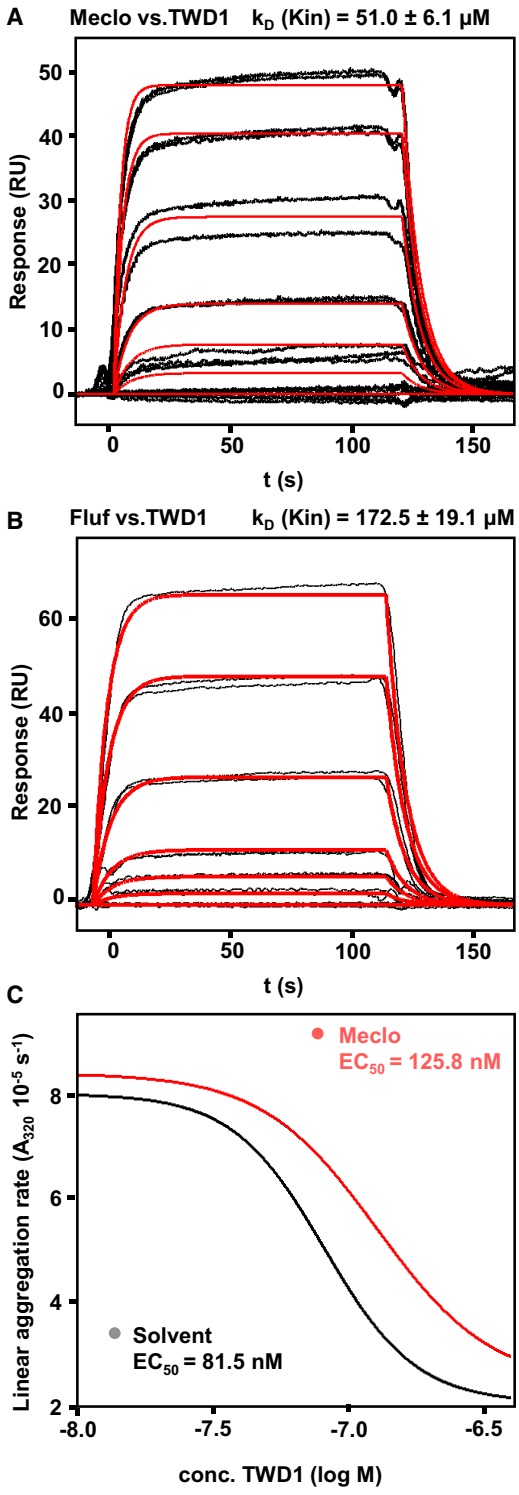

Figure 7. Meclo and Fluf Bind to the FKBD of TWD1 and Alter Its Chaperone Activity

(A and B) Representative kinetic SPR analysis of Meclo (A) and Fluf (B) binding to immobilized TWD1 FKBD protein ($TWD1^{1-180}$) using carboxy-methyldextran (CMD) coupling chemistry. Responses are normalized to a control surface of empty CMD. Kinetic constants were derived by fitting to a Langmuir 1:1 kinetic model with residual deviations and goodness-of-fit indicated in Figures S8A and S8B. RU, normalized response units; n = 3.

(C) Chaperone activity of TWD1 protein assayed by using temperature-induced citrate synthase aggregation (holdase) at 42°C in the presence of solvent or 50 μM Meclo. Citrate synthase concentration was used at 1 μM, recombinant TWD1 was used at indicated concentrations; n = 3.

See also Figures S7 and S8 and Tables S1 and S2.

conducted the *in silico* binding analysis. M. Glanc and P.K. performed the experiments in BY-2 cells in the Petrášek lab. M.D. performed the SPR and TWD1 chaperone activity analyses, and J.L. made mutant *TWD1::TWD1-CFP* constructs in M. Geisler's lab. S.T. and J.F. wrote the manuscript with inputs from M.Glanc, M. Geisler, and other co-authors, and all of the authors revised it.

DECLARATION OF INTERESTS

The authors declare no competing interests.

Received: May 23, 2020
Revised: October 18, 2020
Accepted: November 10, 2020
Published: December 1, 2020

REFERENCES

Adamowski, M., and Friml, J. (2015). PIN-dependent auxin transport: action, regulation, and evolution. Plant Cell *27*, 20–32.

Adamowski, M., Narasimhan, M., Kania, U., Glanc, M., De Jaeger, G., and Friml, J. (2018). A functional study of AUXILIN-LIKE1 and 2, two putative clathrin uncoating factors in *Arabidopsis*. Plant Cell *30*, 700–716.

Armengot, L., Marquès-Bueno, M.M., and Jaillais, Y. (2016). Regulation of polar auxin transport by protein and lipid kinases. J. Exp. Bot. *67*, 4015–4037.

Aryal, B., Laurent, C., and Geisler, M. (2015). Learning from each other: ABC transporter regulation by protein phosphorylation in plant and mammalian systems. Biochem. Soc. Trans. *43*, 966–974.

Benková, E., Michniewicz, M., Sauer, M., Teichmann, T., Seifertová, D., Jürgens, G., and Friml, J. (2003). Local, efflux-dependent auxin gradients as a common module for plant organ formation. Cell *115*, 591–602.

Bouchard, R., Bailly, A., Blakeslee, J.J., Oehring, S.C., Vincenzetti, V., Lee, O.R., Paponov, I., Palme, K., Mancuso, S., Murphy, A.S., et al. (2006). Immunophilin-like TWISTED DWARF1 modulates auxin efflux activities of *Arabidopsis* P-glycoproteins. J. Biol. Chem. *281*, 30603–30612.

Carland, F., Defries, A., Cutler, S., and Nelson, T. (2016). Novel vein patterns in *Arabidopsis* induced by small molecules. Plant Physiol. *170*, 338–353.

Chen, Q., Liu, Y., Maere, S., Lee, E., Van Isterdael, G., Xie, Z., Xuan, W., Lucas, J., Vassileva, V., Kitakura, S., et al. (2015). A coherent transcriptional feed-forward motif model for mediating auxin-sensitive *PIN3* expression during lateral root development. Nat. Commun. *6*, 8821.

Choi, H.W., Tian, M., Manohar, M., Harraz, M.M., Park, S.W., Schroeder, F.C., Snyder, S.H., and Klessig, D.F. (2015). Human GAPDH is a target of aspirin's primary metabolite salicylic acid and its derivatives. PLOS ONE *10*, e0143447.

Choi, H.W., Manohar, M., Manosalva, P., Tian, M., Moreau, M., and Klessig, D.F. (2016). Activation of plant innate immunity by extracellular High Mobility Group Box 3 and its inhibition by salicylic acid. PLOS Pathog. *12*, e1005518.

Cutler, S.R., Ehrhardt, D.W., Griffitts, J.S., and Somerville, C.R. (2000). Random GFP:cDNA fusions enable visualization of subcellular structures in cells of *Arabidopsis* at a high frequency. Proc. Natl. Acad. Sci. USA *97*, 3718–3723.

De Vriese, K., Himschoot, E., Dünser, K., Nguyen, L., Drozdzecki, A., Costa, A., Nowack, M.K., Kleine-Vehn, J., Audenaert, D., Beeckman, T., and Vanneste, S. (2019). Identification of novel inhibitors of auxin-induced Ca2+ signaling via a plant-based chemical screen. Plant Physiol. *180*, 480–496.

Dettmer, J., Hong-Hermesdorf, A., Stierhof, Y.D., and Schumacher, K. (2006). Vacuolar H+-ATPase activity is required for endocytic and secretory trafficking in *Arabidopsis*. Plant Cell *18*, 715–730.

Dhonukshe, P., Grigoriev, I., Fischer, R., Tominaga, M., Robinson, D.G., Hašek, J., Paciorek, T., Petrášek, J., Seifertová, D., Tejos, R., et al. (2008). Auxin transport inhibitors impair vesicle motility and actin cytoskeleton dynamics in diverse eukaryotes. Proc. Natl. Acad. Sci. USA *105*, 4489–4494.

Dindas, J., Becker, D., Roelfsema, M.R.G., Scherzer, S., Bennett, M., and Hedrich, R. (2020). Pitfalls in auxin pharmacology. New Phytol. *227*, 286–292.

Ding, Z., and Friml, J. (2010). Auxin regulates distal stem cell differentiation in *Arabidopsis* roots. Proc. Natl. Acad. Sci. USA *107*, 12046–12051.

Ding, Y., Sun, T., Ao, K., Peng, Y., Zhang, Y., Li, X., and Zhang, Y. (2018). Opposite roles of salicylic acid receptors NPR1 and NPR3/NPR4 in transcriptional regulation of plant immunity. Cell *173*, 1454–1467.e15.

Du, Y., Tejos, R., Beck, M., Himschoot, E., Li, H., Robatzek, S., Vanneste, S., and Friml, J. (2013). Salicylic acid interferes with clathrin-mediated endocytic protein trafficking. Proc. Natl. Acad. Sci. USA *110*, 7946–7951.

Duggan, K.C., Hermanson, D.J., Musee, J., Prusakiewicz, J.J., Scheib, J.L., Carter, B.D., Banerjee, S., Oates, J.A., and Marnett, L.J. (2011). (R)-Profens are substrate-selective inhibitors of endocannabinoid oxygenation by COX-2. Nat. Chem. Biol. *7*, 803–809.

Durrant, W.E., and Dong, X. (2004). Systemic acquired resistance. Annu. Rev. Phytopathol. *42*, 185–209.

Fendrych, M., Akhmanova, M., Merrin, J., Glanc, M., Hagihara, S., Takahashi, K., Uchida, N., Torii, K.U., and Friml, J. (2018). Rapid and reversible root growth inhibition by TIR1 auxin signalling. Nat. Plants *4*, 453–459.

Friml, J., Benková, E., Blilou, I., Wisniewska, J., Hamann, T., Ljung, K., Woody, S., Sandberg, G., Scheres, B., Jürgens, G., and Palme, K. (2002). AtPIN4 mediates sink-driven auxin gradients and root patterning in *Arabidopsis*. Cell *108*, 661–673.

Friml, J., Vieten, A., Sauer, M., Weijers, D., Schwarz, H., Hamann, T., Offringa, R., and Jürgens, G. (2003). Efflux-dependent auxin gradients establish the apical-basal axis of *Arabidopsis*. Nature *426*, 147–153.

Fu, Z.Q., Yan, S., Saleh, A., Wang, W., Ruble, J., Oka, N., Mohan, R., Spoel, S.H., Tada, Y., Zheng, N., and Dong, X. (2012). NPR3 and NPR4 are receptors for the immune signal salicylic acid in plants. Nature *486*, 228–232.

Gallei, M., Luschnig, C., and Friml, J. (2020). Auxin signalling in growth: Schrödinger's cat out of the bag. Curr. Opin. Plant Biol. *53*, 43–49.

Garbers, C., DeLong, A., Deruére, J., Bernasconi, P., and Söll, D. (1996). A mutation in protein phosphatase 2A regulatory subunit A affects auxin transport in *Arabidopsis*. EMBO J. *15*, 2115–2124.

Geisler, M., and Bailly, A. (2007). Tête-à-tête: the function of FKBPs in plant development. Trends Plant Sci. *12*, 465–473.

Geisler, M., Kolukisaoglu, H.U., Bouchard, R., Billion, K., Berger, J., Saal, B., Frangne, N., Koncz-Kalman, Z., Koncz, C., Dudler, R., et al. (2003). TWISTED DWARF1, a unique plasma membrane-anchored immunophilin-like protein, interacts with *Arabidopsis* multidrug resistance-like transporters AtPGP1 and AtPGP19. Mol. Biol. Cell *14*, 4238–4249.

Geisler, M., Blakeslee, J.J., Bouchard, R., Lee, O.R., Vincenzetti, V., Bandyopadhyay, A., Titapiwatanakun, B., Peer, W.A., Bailly, A., Richards, E.L., et al. (2005). Cellular efflux of auxin catalyzed by the *Arabidopsis* MDR/PGP transporter AtPGP1. Plant J. *44*, 179–194.

Geldner, N., Friml, J., Stierhof, Y.D., Jürgens, G., and Palme, K. (2001). Auxin transport inhibitors block PIN1 cycling and vesicle trafficking. Nature *413*, 425–428.

Geldner, N., Anders, N., Wolters, H., Keicher, J., Kornberger, W., Muller, P., Delbarre, A., Ueda, T., Nakano, A., and Jürgens, G. (2003). The *Arabidopsis* GNOM ARF-GEF mediates endosomal recycling, auxin transport, and auxin-dependent plant growth. Cell *112*, 219–230.

Geldner, N., Dénervaud-Tendon, V., Hyman, D.L., Mayer, U., Stierhof, Y.D., and Chory, J. (2009). Rapid, combinatorial analysis of membrane compartments in intact plants with a multicolor marker set. Plant J. *59*, 169–178.

Gilliland, L.U., Pawloski, L.C., Kandasamy, M.K., and Meagher, R.B. (2003). *Arabidopsis* actin gene ACT7 plays an essential role in germination and root growth. Plant J. *33*, 319–328.

Glanc, M., Fendrych, M., and Friml, J. (2018). Mechanistic framework for cell-intrinsic re-establishment of PIN2 polarity after cell division. Nat. Plants *4*, 1082–1088.

Grones, P., and Friml, J. (2015). Auxin transporters and binding proteins at a glance. J. Cell Sci. *128*, 1–7.

Hao, P., Xia, J., Liu, J., Di Donato, M., Pakula, K., Bailly, A., Jasinski, M., and Geisler, M. (2020). Auxin-transporting ABC transporters are defined by a conserved D/E-P motif regulated by a prolylisomerase. J. Biol. Chem. *295*, 13094–13105.

Hardtke, C.S., and Berleth, T. (1998). The *Arabidopsis* gene *MONOPTEROS* encodes a transcription factor mediating embryo axis formation and vascular development. EMBO J. *17*, 1405–1411.

Harper, R.M., Stowe-Evans, E.L., Luesse, D.R., Muto, H., Tatematsu, K., Watahiki, M.K., Yamamoto, K., and Liscum, E. (2000). The *NPH4* locus encodes the auxin response factor ARF7, a conditional regulator of differential growth in aerial *Arabidopsis* tissue. Plant Cell *12*, 757–770.

Hošek, P., Kubeš, M., Lanková, M., Dobrev, P.I., Klíma, P., Kohoutová, M., Petrášek, J., Hoyerová, K., Jiřina, M., and Zazímalová, E. (2012). Auxin transport at cellular level: new insights supported by mathematical modelling. J. Exp. Bot. *63*, 3815–3827.

Kamphausen, T., Fanghänel, J., Neumann, D., Schulz, B., and Rahfeld, J.U. (2002). Characterization of *Arabidopsis thaliana* AtFKBP42 that is membrane-bound and interacts with Hsp90. Plant J. *32*, 263–276.

Kandasamy, M.K., McKinney, E.C., and Meagher, R.B. (2009). A single vegetative actin isovariant overexpressed under the control of multiple regulatory sequences is sufficient for normal *Arabidopsis* development. Plant Cell *21*, 701–718.

Kania, U., Nodzyński, T., Lu, Q., Hicks, G.R., Nerinckx, W., Mishev, K., Peurois, F., Cherfils, J., De Rycke, R., Grones, P., et al. (2018). The inhibitor endosidin 4 targets SEC7 domain-type ARF GTPase exchange factors and interferes with subcellular trafficking in eukaryotes. Plant Cell *30*, 2553–2572.

Katekar, G.F., and Geissler, A.E. (1977). Auxin transport inhibitors: III. Chemical requirements of a class of auxin transport inhibitors. Plant Physiol. *60*, 826–829.

Katekar, G.F., and Geissler, A.E. (1980). Auxin transport inhibitors: IV. Evidence of a common mode of action for a proposed class of auxin transport inhibitors: the phytotropins. Plant Physiol. *66*, 1190–1195.

Kazan, K., and Manners, J.M. (2009). Linking development to defense: auxin in plant-pathogen interactions. Trends Plant Sci. *14*, 373–382.

Keitt, G.W., and Baker, R.A. (1966). Auxin activity of substituted benzoic acids and their effect on polar auxin transport. Plant Physiol. *41*, 1561–1569.

Kieffer, M., Neve, J., and Kepinski, S. (2010). Defining auxin response contexts in plant development. Curr. Opin. Plant Biol. *13*, 12–20.

Kleine-Vehn, J., Dhonukshe, P., Sauer, M., Brewer, P.B., Wiśniewska, J., Paciorek, T., Benková, E., and Friml, J. (2008). ARF GEF-dependent transcytosis and polar delivery of PIN auxin carriers in Arabidopsis. Curr. Biol. *18*, 526–531.

Kleine-Vehn, J., Huang, F., Naramoto, S., Zhang, J., Michniewicz, M., Offringa, R., and Friml, J. (2009). PIN auxin efflux carrier polarity is regulated by PINOID kinase-mediated recruitment into GNOM-independent trafficking in *Arabidopsis*. Plant Cell *21*, 3839–3849.

Klessig, D.F., Tian, M., and Choi, H.W. (2016). Multiple targets of salicylic acid and its derivatives in plants and animals. Front. Immunol. *7*, 206.

Konopka, C.A., Backues, S.K., and Bednarek, S.Y. (2008). Dynamics of *Arabidopsis* dynamin-related protein 1C and a clathrin light chain at the plasma membrane. Plant Cell *20*, 1363–1380.

Kurumbail, R.G., Stevens, A.M., Gierse, J.K., McDonald, J.J., Stegeman, R.A., Pak, J.Y., Gildehaus, D., Miyashiro, J.M., Penning, T.D., Seibert, K., et al. (1996). Structural basis for selective inhibition of cyclooxygenase-2 by anti-inflammatory agents. Nature *384*, 644–648.

Lewis, D.R., and Muday, G.K. (2009). Measurement of auxin transport in *Arabidopsis thaliana*. Nat. Protoc. *4*, 437–451.

Liao, C.-Y., Smet, W., Brunoud, G., Yoshida, S., Vernoux, T., and Weijers, D. (2015). Reporters for sensitive and quantitative measurement of auxin response. Nat. Methods *12*, 207–210, 2, 210.

Lichterman, B.L. (2004). Aspirin: the story of a wonder drug. BMJ *329*, 1408.

Luschnig, C., and Vert, G. (2014). The dynamics of plant plasma membrane proteins: PINs and beyond. Development *141*, 2924–2938.

Luschnig, C., Gaxiola, R.A., Grisafi, P., and Fink, G.R. (1998). EIR1, a root-specific protein involved in auxin transport, is required for gravitropism in *Arabidopsis thaliana*. Genes Dev. *12*, 2175–2187.

Mangoni, A.A., Woodman, R.J., Gaganis, P., Gilbert, A.L., and Knights, K.M. (2010). Use of non-steroidal anti-inflammatory drugs and risk of incident myocardial infarction and heart failure, and all-cause mortality in the Australian veteran community. Br. J. Clin. Pharmacol. *69*, 689–700.

Marc, J., Granger, C.L., Brincat, J., Fisher, D.D., Kao, Th., McCubbin, A.G., and Cyr, R.J. (1998). A *GFP-MAP4* reporter gene for visualizing cortical microtubule rearrangements in living epidermal cells. Plant Cell *10*, 1927–1940.

Marchant, A., Kargul, J., May, S.T., Muller, P., Delbarre, A., Perrot-Rechenmann, C., and Bennett, M.J. (1999). AUX1 regulates root gravitropism in *Arabidopsis* by facilitating auxin uptake within root apical tissues. EMBO J. *18*, 2066–2073.

Michniewicz, M., Zago, M.K., Abas, L., Weijers, D., Schweighofer, A., Meskiene, I., Heisler, M.G., Ohno, C., Zhang, J., Huang, F., et al. (2007). Antagonistic regulation of PIN phosphorylation by PP2A and PINOID directs auxin flux. Cell *130*, 1044–1056.

Mishev, K., Lu, Q., Denoo, B., Peurois, F., Dejonghe, W., Hullaert, J., De Rycke, R., Boeren, S., Bretou, M., De Munck, S., et al. (2018). Nonselective chemical inhibition of Sec7 domain-containing ARF GTPase exchange factors. Plant Cell *30*, 2573–2593.

Mockaitis, K., and Estelle, M. (2008). Auxin receptors and plant development: a new signaling paradigm. Annu. Rev. Cell Dev. Biol. *24*, 55–80.

Nakamura, M., Nishimura, T., and Morita, M.T. (2019). Gravity sensing and signal conversion in plant gravitropism. J. Exp. Bot. *70*, 3495–3506.

Naramoto, S., Otegui, M.S., Kutsuna, N., de Rycke, R., Dainobu, T., Karampelias, M., Fujimoto, M., Feraru, E., Miki, D., Fukuda, H., et al. (2014). Insights into the localization and function of the membrane trafficking regulator GNOM ARF-GEF at the Golgi apparatus in Arabidopsis. Plant Cell *26*, 3062–3076.

Narasimhan, M., Johnson, A., Prizak, R., Kaufmann, W.A., Tan, S., Casillas-Pérez, B., and Friml, J. (2020). Evolutionarily unique mechanistic framework of clathrin-mediated endocytosis in plants. eLife *9*, e52067.

Pasternak, T., Groot, E.P., Kazantsev, F.V., Teale, W., Omelyanchuk, N., Kovrizhnykh, V., Palme, K., and Mironova, V.V. (2019). Salicylic acid affects root meristem patterning via auxin distribution in a concentration-dependent manner. Plant Physiol. *180*, 1725–1739.

Peer, W.A. (2013). From perception to attenuation: auxin signalling and responses. Curr. Opin. Plant Biol. *16*, 561–568.

Petrášek, J., Cerná, A., Schwarzerová, K., Elčkner, M., Morris, D.A., and Zazímalová, E. (2003). Do phytotropins inhibit auxin efflux by impairing vesicle traffic? Plant Physiol. *131*, 254–263.

Petrášek, J., Mravec, J., Bouchard, R., Blakeslee, J.J., Abas, M., Seifertová, D., Wiśniewska, J., Tadele, Z., Kubeš, M., Covanová, M., et al. (2006). PIN proteins perform a rate-limiting function in cellular auxin efflux. Science *312*, 914–918.

Quint, M., and Gray, W.M. (2006). Auxin signaling. Curr. Opin. Plant Biol. *9*, 448–453.

Richter, S., Geldner, N., Schrader, J., Wolters, H., Stierhof, Y.D., Rios, G., Koncz, C., Robinson, D.G., and Jürgens, G. (2007). Functional diversification of closely related ARF-GEFs in protein secretion and recycling. Nature *448*, 488–492.

Richter, S., Kientz, M., Brumm, S., Nielsen, M.E., Park, M., Gavidia, R., Krause, C., Voss, U., Beckmann, H., Mayer, U., et al. (2014). Delivery of endocytosed proteins to the cell-division plane requires change of pathway from recycling to secretion. eLife *3*, e02131.

Robert, S., Chary, S.N., Drakakaki, G., Li, S., Yang, Z., Raikhel, N.V., and Hicks, G.R. (2008). Endosidin1 defines a compartment involved in endocytosis of the brassinosteroid receptor BRI1 and the auxin transporters PIN2 and AUX1. Proc. Natl. Acad. Sci. USA *105*, 8464–8469.

Rong, D., Luo, N., Mollet, J.C., Liu, X., and Yang, Z. (2016). Salicylic acid regulates pollen tip growth through an NPR3/NPR4-independent pathway. Mol. Plant *9*, 1478–1491.

Rouse, D., Mackay, P., Stirnberg, P., Estelle, M., and Leyser, O. (1998). Changes in auxin response from mutations in an *AUX/IAA* gene. Science *279*, 1371–1373.

Ruegger, M., Dewey, E., Hobbie, L., Brown, D., Bernasconi, P., Turner, J., Muday, G., and Estelle, M. (1997). Reduced naphthylphthalamic acid binding in the *tir3* mutant of Arabidopsis is associated with a reduction in polar auxin transport and diverse morphological defects. Plant Cell *9*, 745–757.

Ruegger, M., Dewey, E., Gray, W.M., Hobbie, L., Turner, J., and Estelle, M. (1998). The *TIR1* protein of *Arabidopsis* functions in auxin response and is related to human *SKP2* and yeast *grr1p*. Genes Dev. *12*, 198–207.

Salehin, M., Bagchi, R., and Estelle, M. (2015). SCFTIR1/AFB-based auxin perception: mechanism and role in plant growth and development. Plant Cell *27*, 9–19.

Schindelin, J., Arganda-Carreras, I., Frise, E., Kaynig, V., Longair, M., Pietzsch, T., Preibisch, S., Rueden, C., Saalfeld, S., Schmid, B., et al. (2012). Fiji: an open-source platform for biological-image analysis. Nat. Methods *9*, 676–682.

Schüttelkopf, A.W., and van Aalten, D.M.F. (2004). PRODRG: a tool for high-throughput crystallography of protein-ligand complexes. Acta Crystallogr. Sect. D Biol. Crystallogr. *60*, 1355–1363.

Selinsky, B.S., Gupta, K., Sharkey, C.T., and Loll, P.J. (2001). Structural analysis of NSAID binding by prostaglandin H2 synthase: time-dependent and time-independent inhibitors elicit identical enzyme conformations. Biochemistry *40*, 5172–5180.

Sheahan, M.B., Staiger, C.J., Rose, R.J., and McCurdy, D.W. (2004). A green fluorescent protein fusion to actin-binding domain 2 of *Arabidopsis* fimbrin highlights new features of a dynamic actin cytoskeleton in live plant cells. Plant Physiol. *136*, 3968–3978.

Snyder, W.E. (1949). Some responses of plants to 2,3,5-triiodobenzoic acid. Plant Physiol. *24*, 195–206.

Sondergaard, K.B., and Gislason, G. (2017). NSAIDs and cardiac arrest: non-steroidal anti-inflammatory drug use is associated with increased risk of out-of-hospital cardiac arrest: a nationwide case-time-control study. Eur. Heart J. *38*, 1788–1789.

Swarup, R., Kramer, E.M., Perry, P., Knox, K., Leyser, H.M.O., Haseloff, J., Beemster, G.T.S., Bhalerao, R., and Bennett, M.J. (2005). Root gravitropism requires lateral root cap and epidermal cells for transport and response to a mobile auxin signal. Nat. Cell Biol. *7*, 1057–1065.

Swarup, K., Benková, E., Swarup, R., Casimiro, I., Péret, B., Yang, Y., Parry, G., Nielsen, E., De Smet, I., Vanneste, S., et al. (2008). The auxin influx carrier LAX3 promotes lateral root emergence. Nat. Cell Biol. *10*, 946–954.

Tan, S., Abas, M., Verstraeten, I., Glanc, M., Molnár, G., Hajný, J., Lasák, P., Petřík, I., Russinova, E., Petrášek, J., et al. (2020a). Salicylic acid targets protein phosphatase 2A to attenuate growth in plants. Curr. Biol. *30*, 381–395.e8.

Tan, S., Zhang, X., Kong, W., Yang, X.-L., Molnár, G., Vondráková, Z., Filepová, R., Petrášek, J., Friml, J., and Xue, H.-W. (2020b). The lipid code-dependent phosphoswitch PDK1-D6PK activates PIN-mediated auxin efflux in *Arabidopsis*. Nat. Plants *6*, 556–569.

Tanaka, H., Kitakura, S., De Rycke, R., De Groodt, R., and Friml, J. (2009). Fluorescence imaging-based screen identifies ARF GEF component of early endosomal trafficking. Curr. Biol. *19*, 391–397.

Teale, W., and Palme, K. (2018). Naphthylphthalamic acid and the mechanism of polar auxin transport. J. Exp. Bot. *69*, 303–312.

Trott, O., and Olson, A.J. (2010). AutoDock Vina: improving the speed and accuracy of docking with a new scoring function, efficient optimization, and multithreading. J. Comput. Chem. *31*, 455–461.

von der Fecht-Bartenbach, J., Bogner, M., Krebs, M., Stierhof, Y.D., Schumacher, K., and Ludewig, U. (2007). Function of the anion transporter AtCLC-d in the trans-Golgi network. Plant J. *50*, 466–474.

Walker, V.E., Atanasiu, R., Lam, H., and Shrier, A. (2007). Co-chaperone FKBP38 promotes HERG trafficking. J. Biol. Chem. *282*, 23509–23516.

Wang, Y.S., Motes, C.M., Mohamalawari, D.R., and Blancaflor, E.B. (2004). Green fluorescent protein fusions to *Arabidopsis* fimbrin 1 for spatio-temporal imaging of F-actin dynamics in roots. Cell Motil. Cytoskeleton *59*, 79–93.

Wang, J.-W., Wang, L.-J., Mao, Y.-B., Cai, W.-J., Xue, H.-W., and Chen, X.-Y. (2005). Control of root cap formation by MicroRNA-targeted auxin response factors in *Arabidopsis*. Plant Cell *17*, 2204–2216.

Wang, D., Pajerowska-Mukhtar, K., Culler, A.H., and Dong, X. (2007). Salicylic acid inhibits pathogen growth in plants through repression of the auxin signaling pathway. Curr. Biol. *17*, 1784–1790.

Wang, B., Bailly, A., Zwiewka, M., Henrichs, S., Azzarello, E., Mancuso, S., Maeshima, M., Friml, J., Schulz, A., and Geisler, M. (2013). *Arabidopsis* TWISTED DWARF1 functionally interacts with auxin exporter ABCB1 on the root plasma membrane. Plant Cell *25*, 202–214.

Wang, H.Z., Yang, K.Z., Zou, J.J., Zhu, L.L., Xie, Z.D., Morita, M.T., Tasaka, M., Friml, J., Grotewold, E., Beeckman, T., et al. (2015). Transcriptional regulation of *PIN* genes by FOUR LIPS and MYB88 during *Arabidopsis* root gravitropism. Nat. Commun. *6*, 8822.

Wang, C., Hu, T., Yan, X., Meng, T., Wang, Y., Wang, Q., Zhang, X., Gu, Y., Sánchez-Rodríguez, C., Gadeyne, A., et al. (2016). Differential regulation of clathrin and its adaptor proteins during membrane recruitment for endocytosis. Plant Physiol. *171*, 215–229.

Wang, J., Okkeri, J., Pavic, K., Wang, Z., Kauko, O., Halonen, T., Sarek, G., Ojala, P.M., Rao, Z., Xu, W., and Westermarck, J. (2017). Oncoprotein CIP2A is stabilized via interaction with tumor suppressor PP2A/B56. EMBO Rep. *18*, 437–450.

Wu, G., Otegui, M.S., and Spalding, E.P. (2010). The ER-localized TWD1 immunophilin is necessary for localization of multidrug resistance-like proteins required for polar auxin transport in Arabidopsis roots. Plant Cell *22*, 3295–3304.

Wu, Y., Zhang, D., Chu, J.Y., Boyle, P., Wang, Y., Brindle, I.D., De Luca, V., and Després, C. (2012). The *Arabidopsis* NPR1 protein is a receptor for the plant defense hormone salicylic acid. Cell Rep. *1*, 639–647.

Xu, J., and Scheres, B. (2005). Dissection of *Arabidopsis* ADP-RIBOSYLATION FACTOR 1 function in epidermal cell polarity. Plant Cell *17*, 525–536.

Xu, T., Wen, M., Nagawa, S., Fu, Y., Chen, J.G., Wu, M.J., Perrot-Rechenmann, C., Friml, J., Jones, A.M., and Yang, Z. (2010). Cell surface- and rho GTPase-based auxin signaling controls cellular interdigitation in *Arabidopsis*. Cell *143*, 99–110.

Yin, M.J., Yamamoto, Y., and Gaynor, R.B. (1998). The anti-inflammatory agents aspirin and salicylate inhibit the activity of I(κ)B kinase-β. Nature *396*, 77–80.

Zhang, X., Adamowski, M., Marhava, P., Tan, S., Zhang, Y., Rodriguez, L., Zwiewka, M., Pukyšová, V., Sánchez, A.S., Raxwal, V.K., et al. (2020). *Arabidopsis* Flippases cooperate with ARF GTPase Exchange Factors to regulate the trafficking and polarity of PIN auxin transporters. Plant Cell *32*, 1644–1664.

Zhu, J., Bailly, A., Zwiewka, M., Sovero, V., Di Donato, M., Ge, P., Oehri, J., Aryal, B., Hao, P., Linnert, M., et al. (2016). TWISTED DWARF1 mediates the action of auxin transport inhibitors on actin cytoskeleton dynamics. Plant Cell *28*, 930–948.

Zou, M., Ren, H., and Li, J. (2019). An auxin transport inhibitor targets Villin-mediated actin dynamics to regulate polar auxin transport. Plant Physiol. *181*, 161–178.

STAR★METHODS

KEY RESOURCES TABLE

REAGENT or RESOURCE	SOURCE	IDENTIFIER
Bacterial and Virus Strains		
Escherichia coli DH5α	Lab stock	N/A
Agrobacterium tumefaciens GV3101	Lab stock	N/A
Chemicals, Peptides, and Recombinant Proteins		
Brefeldin A	Sigma	Cat# B7651
Propidium Iodide	Sigma	Cat# P3566
Aspirin	Sigma	Cat# A5376
(S)-(+)-Ibuprofen (dexibuprofen)	Sigma	Cat# 375160
Flurbiprofen	Sigma	Cat# F8514
Ketoprofen	Sigma	Cat# K1751
Naproxen	Sigma	Cat# N8280
Sulindac	Sigma	Cat# S8139
Diclofenac sodium salt	Sigma	Cat# D6899
Indomethacin	Sigma	Cat# I7378
Acetaminophen (Paracetamol)	Sigma	Cat# A7085
Isoxicam	Sigma	Cat# I1762
Phenylbutazone (Bute)	Sigma	Cat# P8386
Mefenamic acid	Sigma	Cat# M4267
Flufenamic acid	Sigma	Cat# F9005
Meclofenamic acid	Sigma	Cat# M4531
Ketorolac (Ketorolac tris salt)	Sigma	Cat# K1136
Piroxicam	Sigma	Cat# P5654
Tenoxicam	Sigma	Cat# T0909
Nimesulide	Sigma	Cat# N1016
Diflunisal	Sigma	Cat# D3281
Murashige & Skoog (MS) Basal Medium including vitamins	Duchefa	Cat# M0222.0050
Benzoic acid (BA)	Sigma	Cat# 242381
Salicylic Acid (SA)	Sigma	Cat# 247588
3-Hydroxybenzoic acid (3-OH-BA)	Sigma	Cat# H20008
4-Hydroxybenzoic acid (4-OH-BA)	Sigma	Cat# H20059
N-(1-Naphthyl)phthalamidic acid (Naptalam, NPA)	Sigma	Cat# N12507
2,3,5-Triiodobenzoic acid (TIBA)	Sigma	Cat# T5910
[^{3}H]-IAA ([5-^{3}H]-Indole-3-acetic acid)	American Radiolabeled Chemicals	Cat# ART 0340
[^{3}H]-NAA ([4-^{3}H]-1-Naphthylacetic acid)	American Radiolabeled Chemicals	Cat# ART 0610
GeneJET Plasmid Miniprep Kit	Thermo Fisher Scientific	Cat# K0503
TWD1-FKBP recombinant protein	(Zhu et al., 2016)	N/A
Deposited Data		
ABCB1 (PGP1)	TAIR	AT2G36910
ABCB19 (PGP19)	TAIR	AT3G28860
TWD1	TAIR	AT3G21640
PIN1	TAIR	AT1G73590
PIN2	TAIR	AT5G57090

(*Continued on next page*)

Continued

REAGENT or RESOURCE	SOURCE	IDENTIFIER
PIP2a	TAIR	AT3G53420
VHA-a1	TAIR	AT2G28520
CLC2	TAIR	AT2G40060
GNL1	TAIR	AT5G39500
ARF1	TAIR	AT2G47170
GNOM	TAIR	AT1G13980
ARA7 (RabF2b)	TAIR	AT4G19640
Experimental Models: Cell Lines		
Nicotiana tabacum L., cv. Bright Yellow-2 (BY-2)	N/A	N/A
Experimental Models: Organisms/Strains		
Arabidopsis thaliana Col-0	Lab stock	N/A
A. thaliana Ws-4	NASC	N5390
A. thaliana twd1-1 (Ws)	(Geisler et al., 2003)	N/A
A. thaliana DR5v2::tdTomato; DR5rev::n3GFP	(Liao et al., 2015)	N/A
A. thaliana DR5rev::GFP	(Friml et al., 2003)	N/A
A. thaliana twd1-3; DR5rev::GFP	This study	N/A
A. thaliana twd1-3 (Col-0)	(Zhu et al., 2016)	N/A
A. thaliana act7-4	(Gilliland et al., 2003; Kandasamy et al., 2009)	N/A
A. thaliana SYP61::SYP61-CFP	(Robert et al., 2008)	N/A
A. thaliana act7-4; SYP61::SYP61-CFP	(Zhu et al., 2016)	N/A
A. thaliana pPIN2::PIN2-GFP; VHA-a1::VHA-a1-mRFP	This study	N/A
A. thaliana twd1-3; pPIN2::PIN2-GFP; VHA-a1::VHA-a1-mRFP	This study	N/A
A. thaliana pVHA-a1::VHA-a1-GFP	(Dettmer et al., 2006)	N/A
A. thaliana pABCB1::ABCB1-GFP	(Dhonukshe et al., 2008)	N/A
A. thaliana pABCB19::ABCB19-GFP	(Dhonukshe et al., 2008)	N/A
A. thaliana 35S::GFP-PIP2a	(Cutler et al., 2000)	N/A
A. thaliana pUBQ10::ARA7-YFP	(Geldner et al., 2009)	N/A
A. thaliana pGNOM::GNOM-GFP	(Geldner et al., 2003)	N/A
A. thaliana HSP::ARF1-GFP	(Xu and Scheres, 2005)	N/A
A. thaliana pGNL1::GNL1-YFP	(Richter et al., 2007)	N/A
A. thaliana 35S::GFP-Fimbrin	(Wang et al., 2004)	N/A
A. thaliana 35S::GFP-fABD2	(Sheahan et al., 2004)	N/A
A. thaliana twd1-1; 35S::GFP-fABD2	(Zhu et al., 2016)	N/A
A. thaliana pCLC2::CLC2-GFP	(Konopka et al., 2008)	N/A
A. thaliana 35S::MAP4-GFP	(Marc et al., 1998)	N/A
A. thaliana twd1-1; 35S::MAP4-GFP	This study	N/A
A. thaliana pPIN2::PIN2-GFP	(Xu and Scheres, 2005)	N/A
A. thaliana pTWD1::TWD1^{K79I}-CFP in *twd1-3*	This study	N/A
A. thaliana pTWD1::TWD1^{H125I}-CFP in *twd1-3*	This study	N/A
A. thaliana pTWD1::TWD1^{K79I}-CFP in Col-0	This study	N/A
A. thaliana pTWD1::TWD1^{H125I}-CFP in Col-0	This study	N/A

(*Continued on next page*)

Continued

REAGENT or RESOURCE	SOURCE	IDENTIFIER
Oligonucleotides		
*twd1-3*_LP: GTGAAGCTGAGGTCTTGGATG	This study	N/A
*twd1-3*_RP: TATGGCCTGAAACAGCAAAAC	This study	N/A
Recombinant DNA		
Plasmid pGreenII0229-pTWD1::TWD1^{K79I}-CFP	This study	N/A
Plasmid pGreenII0229-pTWD1::TWD1^{H125I}-CFP	This study	N/A
Software and Algorithms		
ImageJ	NIH	RRID: SCR_003070; https://imagej.nih.gov/ij/
Fiji	NIH	https://fiji.sc/
ZEN	ZEISS	http://www.zeiss.com/microscopy/int/products.html
GraphPad Prism 8.3.0 (538)	GraphPad	RRID: SCR_002798; https://www.graphpad.com
Origin 2018	OriginLab	https://www.originlab.com/
ACD/ChemSketch	Advanced Chemistry Development, Inc. (ACD/Labs)	https://www.acdlabs.com/resources/freeware/chemsketch/

RESOURCE AVAILABILITY

Lead Contact

Further information and requests for resources and reagents such as plasmids, compounds, mutants, and transgenic lines should be directed to and will be fulfilled by the Lead Contact, Jiří Friml (jiri.friml@ist.ac.at).

Materials Availability

Materials generated in this study, including plasmids, mutants, and transgenic lines, are available on request from the Lead Contact.

Data and Code Availability

The published article includes all analyzed data, and raw data are available upon request from the Lead Contact. This study did not generate any code.

EXPERIMENTAL MODEL AND SUBJECT DETAILS

Plant Materials and Growth Conditions

Arabidopsis thaliana (L.) mutants or transgenic lines used in this study were in the Columbia-0 (Col-0) ecotype background if not specified. The marker lines *pPIN2::PIN2-GFP* (Xu and Scheres, 2005), *pPIN1::PIN1-GFP* (Benková et al., 2003), *DR5v2::tdTomato; DR5rev::n3GFP* (Liao et al., 2015), *DR5rev::GFP* (Friml et al., 2003), *pVHA-a1::VHA-a1-GFP* (Dettmer et al., 2006), *35S::GFP-PIP2a* (Cutler et al., 2000), *pABCB1::ABCB1-GFP* (Dhonukshe et al., 2008), *pABCB19::ABCB19-GFP* (Dhonukshe et al., 2008), *pUBQ10::ARA7-YFP* (*pUBQ10::RabF2b-YFP*) (Geldner et al., 2009), *pGNOM::GNOM-GFP* (Geldner et al., 2003), *HSP::ARF1-GFP* (Xu and Scheres, 2005), *pGNL1::GNL1-YFP* (Richter et al., 2007), *35S::GFP-Fimbrin* (Wang et al., 2004), *35S::GFP-fABD2* (Sheahan et al., 2004), *twd1-1;35S::GFP-fABD2* (Zhu et al., 2016), *act7-4;35S::GFP-fABD2* (Zhu et al., 2016), *pSYP61::SYP61-CFP* (Robert et al., 2008), *act7-4; pSYP61::SYP61-CFP* (Zhu et al., 2016), *pCLC2::CLC2-GFP* (Konopka et al., 2008), *35S::MAP4-GFP* (Marc et al., 1998), *pVHA-a1::VHA-a1-mRFP* (von der Fecht-Bartenbach et al., 2007), and *pPIN2::PIN2-GFP;pVHA-a1::VHA-a1-mRFP* (Naramoto et al., 2014) were reported previously. The mutant *twd1-1* in Wassilewskija (Ws) background was also reported previously (Geisler et al., 2003), and Ws-4 was used as control. *twd1-3;DR5rev::GFP* was made by crossing *twd1-3* and *DR5rev::GFP*. *twd1-1;35S::MAP4-GFP* was made by crossing *twd1-1* and *35S::MAP4-GFP*. All plant lines used in this study are listed in Key Resources Table.

For physiological experiments with *Arabidopsis* seedlings, surface-sterilized seeds were sown on solid Murashige and Skoog (MS) medium [0.5 × MS medium supplemented with 1% (w/v) sucrose, 0.8% (w/v) phytoagar, MES buffer, pH 5.9], kept at 4°C for 2 days'

stratification, and then moved to a growth chamber at 21°C with a 16-h-light/8-h-dark cycle. For microscopic analysis, four-day-old seedlings of different reporter lines were treated with NSAIDs in liquid MS medium. Light sources are GreenPower LED production modules [in deep red (660 nm)/far red (720 nm)/blue (455 nm) combination, Philips], generating a photon density of about 140 μmol/m^2/s (±20%).

METHOD DETAILS

Pharmacological Treatments

For long-term growth experiments, *Arabidopsis* seeds were sown on vertical plates with AM medium plus indicated chemicals, including Benzoic Acid (Sigma, 242381-100G), SA (Sigma, 247588-100G), Aspirin (Sigma, A5376-100G), Ibuprofen (Sigma, 375160-5G), Indometacin (I7378-10G), Sulindac (Sigma, S8139-5G), Naproxen (Sigma, N8280-5G), Ketoprofen (Sigma, K1751-5G), Ketorolac tris salt (Sigma, K1136-1G), Flurbiprofen (Sigma, F8514-1G), Flufenamic Acid (Sigma, F9005-10G), Mefenamic Acicd (Sigma, M4267-50G), Meclofenamic Acid (Sigma, M4531-1G), Isoxicam (Sigma, I1762-1G), Piroxicam (Sigma, P5654-1G), Tenoxicam (Sigma, T0909-250MG), Nimesulide (Sigma, N1016-1G), Diflunisal (Sigma, D3281-5G), Acetaminophen (Sigma, A7085-100G), NPA (Sigma, N12507-250MG), TIBA (Sigma, T5910-5G), and Diclofenac sodium salt (Sigma, D6899-10G). After 2-d stratification, plants were transferred to a growth chamber as mentioned in the ''Plant material and growth conditions'' session, for 7 days or 10 days. For short-term treatment, 4-day-old seedlings were incubated in liquid AM medium with indicated chemicals for indicated time course. Details are described below for each treatment or staining series. All chemicals used in this study are listed in Key Resources Table.

Auxin transport assays in *Arabidopsis* hypocotyls and tobacco BY-2 cells

The rootward (basipetal) transport of [^{3}H]-IAA with intact *Arabidopsis* hypocotyls was performed as reported previously (Lewis and Muday, 2009; Tan et al., 2020b), with a few modifications. 6-day-old etiolated Col-0 seedlings were transferred to new MS plates with different NSAIDs (1 h pretreatment, with DMSO as the solvent control). 15 seedlings were pooled as one biological replicate, with 4 replicates for each genotype. Agarose droplets with [^{3}H]-IAA (PerkinElmer) were prepared in MS medium with 1.25% (w/v) agarose, indicated NSAIDs, and 125 μM [^{3}H]-IAA (1.45 μL in 10 mL this solution), 10 μL/droplet on a Petri-dish. Then [^{3}H]-IAA droplets were placed at the shootward end of decapitated seedlings. After 6 hours' incubation in the darkness, the lower part of the hypocotyls were cut, collected into a 2-mL Eppendorf tube (with two iron beads inside), and then frozen in liquid nitrogen. The samples were ground completely and then homogenized in 1 mL scintillation liquid (PerkinElmer). Eventually the radioactivity of ^{3}H was measured with a scintillation counter (Hidex 300XL), with each sample counted for 300 s, 3 times. Three scintillation solution controls were used for subtraction in data analysis.

[^{3}H]-NAA transport assays in BY-2 cells were performed as described previously (Petrášek et al., 2006). Cells were pretreated with indicated chemicals for 20 s before the measurement.

Imaging by confocal laser scanning microscopy (CLSM)

Fluorescence imaging was performed using a Zeiss LSM800 confocal laser scanning microscope with a GaAsP detector (Zeiss, Germany). The manufacturer's default settings (smart mode) were used for GFP (excitation, 488 nm; emission, 495-545 nm)-, RFP (excitation, 561 nm; emission, 580-650nm)-, YFP (excitation, 514 nm; emission, 524-580nm), tdTomato (excitation 561 nm; emission, 571-630 nm), and Venus (excitation, 514 nm; emission, 524-580 nm)-tagged proteins. To image FM4-64-stained cells, a laser line of 543 nm was used for excitation, and an emission light with a wavelength of 600-700 nm was collected. For PI staining, excitation, 561 nm; emission, 580-680 nm. All images were taken in 8 bit depth, 2 × line averaging. For time-lapse imaging, 8 bit depth, 2 × line averaging.

For BFA washout experiments, four-day-old *Arabidopsis* seedlings were incubated in liquid medium and treated with 37.5 μM BFA for 60 min and quickly washed three times with the normal medium. The treated seedlings were then transferred to normal liquid medium containing 0.1% (v/v) DMSO or indicated concentrations of NSAIDs and recovered for 120 min before imaging with confocal microscopy.

FM4-64 uptake assays and PI staining

To study the effects of NSAIDs on endocytosis, one lipophilic fluorescent dye FM4-64 [N-(3-Triethylammoniumpropyl)-4-(6-(4-(Diethylamino) Phenyl) Hexatrienyl) Pyridinium Dibromide, Life Technology, T-13320] was used to examine this. Four-day-old *Arabidopsis* seedlings were incubated in liquid medium with NSAIDs for 30 min, and then added FM4-64 at the final concentration of 2 μM for incubation 15 min before imaging with CLSM (Zeiss LSM800).

PI (Propidium iodide, 1 mg/mL stock solution, Thermo Fisher Scientific, P3566) staining was performed for roots as reported previously (Tan et al., 2020b). In detail, four-day-old *Arabidopsis* seedlings were incubated in liquid MS medium with NSAIDs, TIBA, or DMSO (solvent control) for 30 min, and then stained with PI (diluted in H_2O) at the final concentration of 10 mg/L for 1 min before imaging with CLSM (Zeiss LSM800).

Startolith starch staining with Lugol's solution

Five-day-old *Arabidopsis* Col-0 seedlings were stained with Lugol's solution (Sigma) 2 min, and then washed with liquid MS medium for 2 min, as previously reported (Tan et al., 2020b). Whole seedlings were mounted on a slide with a clearing solution (30 mL H_2O, 10 mL glycerol, 80 g chloral hydrate, with 100 mL in total), and then covered with a coverslip. Eventually, root tips were imaged with a differential interference contrast (DIC) microscopy (Olympus BX53).

Image analysis and morphological analysis

For primary root length measurement, plates with *Arabidopsis* seedlings were imaged with a scanner (Epson Perfection V800 Photo) or a camera (Sony A600 with a macro lens), and then the primary root length or root tip angles were analyzed with ImageJ (Schindelin et al., 2012). Lateral root numbers were counted directly.

In silico substrate docking analysis and quantum chemical modeling for NSAIDs and TWD1

In silico substrate docking and quantum chemical modeling were performed as reported previously (Zhu et al., 2016). In short, for *in silico* substrate docking, one thousand poses for each PRODRG-generated (Schüttelkopf and van Aalten, 2004) NSAID structure files were docked onto TWD1 FKBD structures (PDB accession codes 2F4E and 2IF4) using the PyMOL-embedded AutoDock Vina toolset (Trott and Olson, 2010). Search space was first defined as the whole rigid FKBP structure with high exhaustiveness and further refined to the TWD1 FKBD NPA site in flexible side-chain mode (P_{37}PKKVDS-Q_{54}II-R_{75}AWTK-S_{81}QH-A_{122}LVH-L_{149}LYEV). The calculations resulted in 8 to 20 clusters with close conformations. For quantum chemical modeling, NSAIDs and NPA were analyzed with the same methods as reported before (Zhu et al., 2016), for the geometry, electronic structure and electronic binding energies to the proposed NPA binding sites.

Surface plasmon resonance (SPR) analysis

Recombinant TWD1 FKBD (aa 1-339) protein was published before, and SPR analysis was performed as reported previously (Zhu et al., 2016). In detail, the TWD1 FKBD protein was prepared in 10 mM sodium acetate pH 5 and immobilised to approximately 20 uRIU on a derivatized carboxymethyl dextran (CMD) sensor chip (CMD500m, XanTec Bioanalytics GmbH, Düsseldorf, Germany) by covalent thiole-coupling of accessible cysteine residues according to manufacturer's instructions. Stock solutions and serial dilutions of NSAIDs were prepared in ethanol and diluted in running buffer (10mM HEPES, 50mM NaCl, 10mM $MgCl_2$, 10mM KCl, 0.05% (v/v) Tween-20, pH 7.6) for analysis. The SPR system was equilibrated with running buffer supplemented 1% (v/v) ethanol. All experiments were conducted at 25°C and included blank injections (running buffer + 1% ethanol) for double referencing. At least two independent dilutions of NSAIDs for each of the indicated concentrations were injected in duplicates, first over the TWD1 FKBD coupled surface and subsequently over a L-cysteine blocked reference surface. Acquired data was processed with Scrubber3 and Tracedrawer software as described previously for determination of kinetic parameters (Zhu et al., 2016).

TWD1 chaperone activity assay

Citrate synthase was used as a substrate for TWD 1 chaperone activity. TWD1 was assayed chaperone activity according to a previous publication (Kamphausen et al., 2002) with a few modifications. The aggregation of 375 nM Citrate synthase, in the presence of variable concentrations of the TWD1 FKBD chaperone (Zhu et al., 2016) and 50 uM Meclofenamic acid or 0.1% DMSO solvent control, was assayed at 55°C by measuring time dependent changes in light scattering/optical density at 320 nm in a multi-well format using UV-transparent 96-well plates (Product information) and a Cytation 5 plate reader (BioTek Instruments). The assay buffer consisted of 50 mM HEPES, and 100 mM NaCl pH 7.6. Control measurements for the aggregation of TWD1 were carried out in the absence of citrate synthase. Blank measurements were carried out using assay buffer with and without Meclofenamic acid as applicable and used to reference acquired data. Aggregation rates were calculated by linear regression of the linear portion of the aggregation curves.

Accession numbers

Published sequence data from this article can be found in the *Arabidopsis* Genome Initiative or enBank/EMBL databases. Here are the accession numbers: ABCB1 (PGP1, AT2G36910), ABCB19 (PGP19, AT3G28860), TWD1 (AT3G21640), PIN1 (AT1G73590), PIN2 (AT5G57090), PIP2a (AT3G53420), VHA-a1 (AT2G28520), CLC2 (AT2G40060), GNL1 (AT5G39500), ARF1 (AT2G47170), GNOM (AT1G13980), and ARA7 (RabF2b, AT4G19640).

QUANTIFICATION AND STATISTICAL ANALYSIS

Most experiments have been repeated at least three times independently, with similar results obtained. For measurements of primary root length and root tip angles, photos or scans were analyzed with the ImageJ program (https://imagej.nih.gov/ij/download.html). Fluorescence intensity for CLSM images was quantified by Fiji (https://fiji.sc/) (Schindelin et al., 2012). Data visualization and statistics were mostly performed with Graphpad Prism8. For bending curvatures of roots tips, polar graphs were generated by Origin 2018. *n* and *p* values are indicated in figures or legends.